Geochemistry, Geophysics, Geosystems
November 2008; Volume 9 (Q11R05) : NIL_40-NIL_66
http://dx.doi.org/10.1029/2007GC001854

An edited version of this paper was published by AGU.

The 100-ka and rapid sea level changes recorded by prograding shelf sand bodies in the Gulf of Lions (western Mediterranean Sea)

M.A. Bassetti[1, 2, *], S. Berné[1, 2], G. Jouet[2], M. Taviani[3], B. Dennielou[2], J.-A. Flores[4], A. Gaillot[5], R. Gelfort[6], S. Lafuerza[7], N. Sultan[2]

[1] Université de Perpignan IMAGES, 52 avenue Paul Alduy, Perpignan, France
[2] IFREMER, Géosciences Marines, BP70, 29280 Plouzané, France,
[3] ISMAR/CNR via Gobetti 101, Bologna, Italy
[4] Universidad de Salamanca, Facultad de Ciencias, Plaza Merced s/n, Salamanca, Spain,
[5] ALTRAN OUEST, Technopole Brest Iroise, CS 23866, 29238 Brest, Cedex 3, France
[6] Institut für Geowissenschaftliche Gemeinschaftsaufgaben (GGA), Stilleweg 2, 30655, Hannover, Germany
[7] GRC Geociències Marines, Departament d'Estratigrafia i Paleontologia I Geociències Marines, Universitat de Barcelona, Martí i Franquès s/n, 08028 Barcelona, Spain

*: Corresponding author : Bassetti M.A., email address : maria-angela.bassetti@univ-perp.fr

Abstract:

Thick forced regressive units on the wide continental shelf of the Gulf of Lions (western Mediterranean) recorded the composite effect of sea level changes during the Quaternary. They are mostly composed of coastal siliciclastic and bioclastic wedges showing clinoform geometry. These deposits have been intensively explored through high-resolution seismic investigations, but only recently it was possible to ground truth seismic interpretations, based on a long (100 m) borehole that crossed the succession and recovered a large part of the mainly sandy deposits (84% recovery). A multiproxy analysis of the sedimentary succession shows that (1) the stratal architecture of the shelf margin is defined by major bounding surfaces that are polygenic erosion surfaces associated with coarse-grained material incorporating abundant and diverse shells, including cold-water fauna (presently absent from the Mediterranean Sea). Between each surface, coarsening upward units with steep (up to 5°) foresets are made of massive (more than 20 m thick) sands with possible swaley and hummocky cross-stratification, passing seaward to sands with muddy intervals and, further offshore, alternating highly boiturbated sands and silts. Each prograding wedge corresponds to a forced-regressive shoreface (or delta front/prodelta), deposited during the overall sea level falls occurring at (relatively slow) interglacial/glacial transition and therefore represents the record of 100 ka cyclicity. Higher-frequency Milankovitch cyclicities are also probably represented by distinct shoreface/delta front wedges; (2) detailed examination of the architecture and chronostratigraphy of the most recent sequence shows that minor bounding surfaces, corresponding to abrupt shallowing of sedimentary facies, separate downward stepping parasequences within the last 100 ka sequence. These events are in phase with millennial-scale glacial climatic and sea level variability, the downward shift surfaces corresponding to the falls during the coldest stadials. These deposits provide a comprehensive and well-constrained Pleistocene analog to the numerous shoreface deposits attributed to falling-stage systems tracts recognized in ancient stratigraphic records, studied at the outcrop scale.

1. Introduction

Prograding beach-shoreface deposits are a common component of the stratigraphic record [Walker and Plint, 1992]. They correspond to one of the key “facies models” utilised by sedimentologists studying the stratigraphic record, and the analysis of their evolution through time is at the origin of most sequence-stratigraphic paradigms [Posamentier et al., 1992]. Beach-shoreface deposits are very sensitive to base-level changes, thus they have been also utilized, under certain conditions, as “dipsticks” for sea-level changes [Rabineau et al., 2006]. In addition, because of their high content of well-sorted sand, they also represent potential reservoirs for hydrocarbons. However, the shallow marine processes that are recorded in detail within shorefaceforeshore- shelf parasequences are barely known. This is mostly due to the lack of lithological data on Quaternary shoreface deposits, which are mainly known through high-resolution seismic investigations or from interpretation of outcrops examples of ancient shoreface deposits. The term “shoreface” is used here in the sense of van Wagoner et al. [1990], i.e. sediments deposited between the foreshore and the storm wave base. In a wave-dominated deltaic setting, it corresponds to the delta front and prodelta domains, and it is generally difficult, in the stratigraphic record, to make the distinction between both settings, especially when longshore drift modifies the geometry of sand bodies [Bhattacharya and Giosan, 2003]. The Gulf of Lions, in the NW Mediterranean Sea has been the subject of intense high-resolution seismic investigations during the last 10 years [Berné et al., 2004]. Because of high sediment supply and rapid subsidence it offers an exceptional record

of shelf/slope sequences linked to glacio-eustatic sea-level changes during the last 500 ky. However, attempts to core the sand bodies deposits that constitute one of the key component of the shelf/slope succession was largely unsuccessful, due to the presence of coarse shell lags making piston and vibra-coring operations very difficult. The maximum recovery using these conventional techniques were cores about 2.5 m long [*Aloïsi*, 1986; *Bassetti et al.*, 2006; *Berné et al.*, 1998]. For similar reasons, ODP leg 174A on the New Jersey continental shelf encountered great difficulties recovering, with "Advanced Piston Coring", the sandy successions that constitute most of Quaternary deposits on this margin [*Austin et al.*, 1998]. Similarly, attempts to core a sand ridge in the North Sea experienced major difficulties, with an overall recovery less than 16% [*Davis and Balson*, 1992]. The most comprehensive investigation of sandy clinoforms was conducted by a consortium of oil companies, which successfully drilled shelf-edge deltas of the Mississippi margin [*Winn et al.*, 1995]. However, the borehole described by these authors is located beyond the shelf edge, and the authors do not provide description of sedimentary facies within the clinoform units.

In June-July 2004, a drilling operation was funded by the European Community in order to investigate the Adriatic and the Gulf of Lions deltaic margins (PROMESS 1-PROfiles across MEditerranean Sedimentary Systems). Two sites were drilled in the Gulf of Lions: PRGL1- 4 (300 m long), located at the interfluves of Bourcart and Herault canyons at a water depth of 298 m, and PRGL2-2 (100 m long, 103 m water depth), through the seaward termination of a preserved last glacial shoreline (Figure 1). In particular, PRGL2-2 drilled through sedimentary discontinuities related to submarine and/or subaerial erosion that can be tied to correlative conformities towards the slope. The borehole provided valuable information on seismic and sedimentary facies, as well as physical and geotechnical properties.

Interpretations of the prograding sediment wedges that were drilled during the cruise at site PRGL2-2 are here provided, since the drilling operations were successfully terminated with the satisfactory core recovery of 84%, despite the presence of thick sandy intervals. The correspondence between sedimentary and seismic facies is here demonstrated, thanks to the newly acquired sedimentological data that permit detailed characterization the seismic response to lithological changes. For intervals

with no recovery, lithologies were predicted from Cone Penetration Test [*Lafuerza et al.*, this volume].

The major objectives of our study are:

- To describe the sedimentary facies of clinothem units, and to interpret their depositional environment;
- Understanding how the different facies and sequences record the changing sea-level and how important surfaces can be recognized from subsurface and sedimentological data.

2. Regional setting

The Gulf of Lions is a passive, prograding and subsiding margin, located in the north-western sector of the Mediterranean Sea bounded, to the west and east, by Pyrenean and Alpine orogenic belts, respectively (see the synthesis by *Berné and Gorini* [2005]). It comprises a wide (about 70 km) shelf and a continental slope that is incised by numerous canyons descending to the abyssal area of the Algero-Balearic Basin. Because of high sediment supply (mainly from the Alps through the Rhône River) and very limited tectonic activity, the Gulf of Lions is a favourable environment for studying the deposition and preservation of sequences controlled by glacio-eustasy.

During the last ca. 500 ky, sea level oscillated between its present position and about 120 m below the present sea level. Because the shelf edge is located between 105 and 165 m water depth, a large portion of the continental shelf was exposed during glacial periods. As a result, the stratigraphic record displays major erosional surfaces resulting from subaerial and shallow marine erosion during sea-level falls, lowstands and sea-level rises.

The cyclically stacked Plio-Quaternary sequences have been object of seismic investigations over the last 30 years by several authors who proposed a number of conceptual and/or numerical stratigraphic models [*Aloïsi*, 1986; *Berné et al.*, 1998; 2004; *Lofi et al.*, 2003; *Monaco*, 1971; *Rabineau et al.*, 2005; *Tesson et al.*, 1990; 2000]. A review of these investigations is given by *Rabineau et al.* [2005]. Most of the middle and outer continental shelf consists of prograding wedges that display internal reflections showing alternating low angle (<1°) and high angle (>4°) clinoforms. Based on shallow cores and stratigraphic modelling, this elementary "motif" was interpreted as the result of alternating deposition of high energy (sandy

upper shorefaces/delta fronts) and low energy (muddy lower shorefaces or “offshore” deposits) during late Quaternary sea-level changes. The large (>100 km) lateral extent of these sand bodies suggest a global (sea-level) control on their deposition. However, the nature of the prograding shorefaces remained controversial; some authors interpreted them as the product of deposition during the falling stage of sea-level [*Aloïsi,* 1986; *Berné et al.,* 1998; *Rabineau et al.,* 2005] whereas others proposed that they could correspond to transgressive parasequences (in the sense of *Van Wagooner et al.* [1990]) formed during the early stages of sea-level rises [*Tesson et al.,* 2000]. Also, the formation timing of these deposits remained elusive, with some authors interpreting the major bounding surfaces separating each prograding unit as sequence boundaries linked to the 100 ky glacial/interglacial cycles [*Aloïsi,* 1986; *Lobo et al.,* 2005; *Rabineau,* 2001], whereas others ascribed them to higher-order (20ky) cyclicities [*Tesson et al.,* 1993; 2000].

3. Methods

The data were collected onboard SRV “Bavenit” of the Russian company “Amige”, operated by Fugro. In order to evaluate sediment types to be cored, and for geotechnical characterisation, we first performed a continuous CPTU (Cone Penetration Test Unified) at site PRGL2-1, distant a few m from the PRGL2-2 site where continuous coring was carried out. The test was made with a static penetrometer measuring:

- cone resistance (kPa);
- sleeve friction (kPa);
- pore pressure acting on the cone (kPa).

The CPTU equipment and the procedures adopted during the cruise operations are in accordance with the International Reference Test Procedure published by the Society of Soil Mechanisms and Geotechnical Engineering (ISSMGE, 1999). Estimation of sediment types based on geotechnical properties was done using the method of Soil Classification established after *Ramsey* [2002].

An important application of CPTU measurements is the prediction of the stratigraphy and lithology of buried sediments. Thanks to the combination of three CPTU measurements (cone resistance, lateral friction, pore pressure, [*Ramsey,* 2002]) it is possible to define the soil type based on a soil classification chart (see details in *Lafuerza et al.,* this volume). It relies on a large CPTU database adapted and

improved by different authors to diagrams of soil classification [*Ramsey*, 2002; *Robertson*, 1990].

All geotechnical data were combined for soil characterization, considering that the pore pressure (u_2) is mainly related to the permeability of sediments, whereas the resistance to cone penetration (*qt*) and the lateral friction (*fs*) can be directly correlated to a particular lithology.

Core sections, from 0.80 to 1.5 m in length, were recovered using a suite of FUGRO corers, including a piston corer, a "WIP" corer and a FUGRO corer. Overall, about 50% of the drilled section consisted of sand, making core recovery difficult. However, within very sandy intervals, the strategy consisted to core down to the maximum of penetration, then, when core recovery was less than 50 cm, to drill only 50 cm in order to minimize the gaps. This time-consuming operation allowed overall recovery of 84%.

Physical properties of collected cores were measured onboard using a GEOTEK Multi-Sensor Core Logger (MSCL), by means of:

- gamma-ray density;
- P-wave velocity;
- magnetic susceptibility.

Magnetic susceptibility was measured a second time in the laboratory on split cores. To link lithological, seismic and geotechnical data, a time-depth conversion was constructed using P-wave velocities from MSCL. From this calculation, all logs were converted into a time scale (ms, Two Way Travel Time, TWTT). In addition, velocities of fine-grained intervals were measured using a pair of transducers oriented along the core axis. The very good match between major lithological changes and boundaries of seismic units demonstrates the validity of the method.

All cores were visually described, and X-ray images were realized for the most significant sections. The X-ray radiography was particularly useful for enhancing subtle sedimentary structures not easily identified on freshly-cut core surfaces.

Measurements of carbonate content (Bernard calcimeter, precision ±2%) and grain size analyses with a laser microgranulometer (Coulter counter LS130; size range 0.4 μm to 1 mm) were made on the total sediment fraction on samples collected every 20 cm (with the exception of gravel beds).

In order to establish a biostratigraphic control, the cores were analysed onboard for calcareous nannoplankton [*Colmenero and Gravalosa*, personal communication], additional samples being analysed after core splitting in the laboratory.

The chronostratigraphy of the youngest sequence is based on AMS ^{14}C dating of biogenic carbonates (mainly Foraminifera). In addition, attempts were made on a few samples to date total organic carbon or wood fragments. Approximately 10 mg of biogenic carbonate was handpicked under the binocular microscope and AMS ^{14}C dates were obtained by the Poznan Radiocarbon Laboratory of the Adam Mickiewicz University (Poland). All ages reported here are given in calibrated ages. For ages between 0 and 21,880 ^{14}C BP calendar (i.e. calibrated) ages were calculated using correction tables [*Stuiver and Reimer,* 1993] and by mean of Calib 5.0.2 sofware (http://calib.qub.ac.uk/calib/). For the marine material, the Marine04 calibration curve [*Hughen and al.,* 2004; *Reimer et al.*, 2004] was used with no deviation from the mean global reservoir correction (-400 y). For continental material the Intcal04 calibration curve [*Reimer et al.*, 2004] was used. For ages beyond 21,880 ^{14}C BP, the Glacial Polynomial [*Bard et al.*, 1998] was used. Calendar ages are given with 1 sigma standard error.

Beyond the radiocarbon dating resolution, chronostratigraphy was obtained by estimations of the abundance of biostratigraphically significant coccolith taxa, following the criteria of *Raffi and Flores* [1995].

In addition to core data, spectral gamma ray measurements were performed in situ by means of wireline logging. Total gamma counts and Potassium (^{40}K), Thorium (^{232}Th) and Uranium (^{238}U) fractions were recorded. Because open hole logging was deemed to be too risky in such unconsolidated marine sediments, logging took place within the drill string and bottom hole assembly (BHA). While this ensured a safe operation, gamma counts were severely diminished by the surrounding steel. From the BHA design, steel thicknesses were established and data corrected for using the ENCOR algorithm as developed by *Hendriks* [2003]. Spectral gamma ray results showed no major features but total gamma ray counts were utilised as clean sand vs. clay indicator.

4. Results

4.1. Seismic sequences and surfaces

The overall seismic stratigraphic organization of the shelf/upper slope is summarized in Figure 2. In the Gulf of Lions margin, prograding wedges, attributed to forced-regressive systems tracts [*Hunt and Tucker*, 1992] thicken seaward. These wedges are bounded by erosion surfaces that become correlative conformities on the upper continental slope, where they have been precisely dated. They form a hierarchy of bounding surfaces in the sense of *Brookfield* [1977].

Major seismic surfaces are traceable throughout the Gulf of Lions and they correspond to 100 ky glacio-eustatic cycles [*Rabineau et al*., 2005]. They bound major seismic units. ***Minor seismic surfaces*** have not been correlated at the regional scale [*Jouet*, 2007], but display an erosional geometry, or distinct changes in clinoform geometries, within major seismic units. These minor surfaces have been correlated to distinct and well-dated climatic/sea-level events identified in long piston cores [*Jouet et al.*, 2006] or in the PROMESS 1 drill sites.

In the vicinity of PRGL2-2, seismic facies seen on multi-channel and sparker profiles (Figure 3) are characterized by various clinoform geometries. From the top to the bottom of the borehole, 6 major seismic units are identified (see further details in the Auxiliary Material):

- Unit U150 is characterized by steep (up to 5°) clinoforms pinching out seaward and forming a ~48 ms (42 m) thick wedge interpreted as a forced regressive and lowstand shoreface [*Rabineau et al.*, 2006]. Cemented sands (C.S. in Figure 3), interpreted as beach rocks by *Berné et al.* [1998] and *Jouet et al.* [2006] are exposed on the sea-floor 1 km south of the drill site (Figure 3). Within U150, several minor bounding surfaces identified on the Bourcart-Hérault interfluve [*Jouet et al.*, 2006] have been recognized here in this proximal depositional environment. At PRGL2-2 position, D63 is an erosion surface dated between 41 and 38 cal ky BP [*Jouet et al*., 2006]. D64 and D65 display more subtle changes, but theses surfaces are traceable in a strike direction for over 15 km (D64) and across the entire shelf edge (D65) [*Jouet*, 2007]. These bottomsets form the downlap surface for high-angle clinoforms deposited subsequently (Figure 3). These minor bounding surfaces allow the identification, within U150, of four seismic sub-units, labelled U147, U151a, U151b, U152 (Figure 3) [*Jouet et al.*, 2006]. In addition, a sub-horizontal minor bounding surface truncates the upper part of the clinoforms of U150. A large number of shallow cores and ultra-high resolution seismic profiles have shown that it is a *ravinement* surface dated between 15 and 16 cal ky BP (at 99 m water depth), that

formed during the last deglacial sea-level rise [*Bassetti et al.*, 2006]. Locally, this surface underlies elongated sand bodies (unit 155 of Figure 3), several km long, some hundred meters wide and 5-10 m thick, oriented NW-SE and interpreted as transgressive sand ridges [*Bassetti et al.*, 2006].

- **Unit U129** is a seaward-thickening wedge made of very low-angle clinoforms (high-amplitude, parallel reflections). Its upper termination (D60) is an erosion surface (see left-hand side of Figure 3B) that seaward becomes a correlative conformity.

- **Unit U100** displays continuous, low-angle clinoforms shaped, seaward of unit 80, into wavy structures, that could be interpreted either as submarine retrogressive slides or, more likely, sediment waves (see the review by *Lee et al.* [2002]). These structures are asymmetrical with a steep side facing upslope, suggesting landward migration if they are sediment waves. In 3 dimensions, this unit also displays 3 sub-units [*Rabineau et al.*, 2005].

- **Unit U80** displays seismic facies similar to that of U151/152 at PRGL2-2 position, with clinoforms dipping at angles up to 5°, but the topsets are better preserved as in U151/152 and their sigmoid shape is clearly visible (Figure 3).

Below these prisms, several major erosion bounding surfaces are observed at the position of PRGL2-2 (D45, D40, D35 and D30). D45-40-35 corresponds to 3 erosion surfaces, amalgamated on the shelf and that separate seaward (Figure 2). Hereafter, it will be named D45 (Figure 3). Between these erosion surfaces, **Unit U57** is a <5 m-thick seismic unit, difficult to correlate laterally. The bottom of the borehole reached seismic **Unit U40** that corresponds to the infill of an axial incision (in the sense of *Baztan et al.* [2005]) cutting across a major buried canyon connected to the present Bourcart Canyon (Figure 1).

4.2- Lithology, bio- and sedimentary facies of seismic units

PRGL2-2 offers a unique opportunity to verify the actual nature of sandy clinoforms that have been imaged all around the world but almost never sampled with satisfying recovery.

At the core scale, 14 sedimentary units were identified on the basis of their sedimentary facies (Table 1, Auxiliary Material). They are bounded by 5 coarse-grained intervals, the positions of which perfectly correspond to the 5 major

bounding surfaces (D70, D60, D50, D45, D30) previously described on seismic profiles (Figure 4). The detailed lithological description of the borehole is included in the Auxiliary Material section, as well as the geotechnical properties (Figure 5) that were utilized to interpolate with good confidence the lithological information for non-recovered intervals.

- **U152** is an overall coarsening upward sequence as defined on the basis of lithology, grain size and Gamma ray (**sedimentary unit 1;** Figures 4, 6). This unit is topped by a coarse to medium sand interval, 1.90 m thick, with shell debris (D70). It displays laminated or cross-bedded well-sorted and homogeneous fine- to medium-grained sand, with scattered rounded pebbles. Thin (1-2 cm) mud interbeds occur within the lower part of this interval (Figure 7, sections 8A, 10A, 14A; Figure 9.1). Swaley cross-stratification [*Leckie and Walker*, 1982] or hummocky cross stratification [*Harms et al.*, 1975] can be inferred at levels (Figure 7, section 14A) but these large-scale sedimentary structures are not easy to recognize at core scale.

- **U151 (sedimentary unit 2)** is also a coarsening upward sequence consisting of mud-sand alternations with mm-thick sandy beds, laminated and intensely burrowed, separated by 1 to 10 cm-thick muddy beds (Figures 9.2; 9.3; 9.4). The bottom of unit 2 is marked by a very distinct transition toward massive silty clay with sparse bioturbation, and a carbonate content > 25% (Figure 6). In detail, this unit can be divided into 4 coarsening-upward sub-units, each displaying a coarsening upward pattern (Figure 11A).

Seismic units U151 and U152 are characterized by a very poor faunal content. Rare worn fragments of bivalves are found together with partly reworked benthic foraminifera (mainly *Ammonia* sp. and *Elphidium* sp., Figure 10)

- **Surface D60** corresponds to 80 cm of very coarse-grained material, mainly composed of shell fragments **(sedimentary unit 3)**. In detail, 2 coarse-grained intervals with an erosional base can be distinguished, separated by less than 10 cm of marine clay (Figure 11B). This interval is rich in molluscs but with low-diversity faunal assemblage dominated by *Abra* sp., *Corbula* sp. and *Turritella communis* (Figure 10)

- **U129 (Sedimentary unit 4)** is made of alternating beds of fine sand and bioturbated clay or silty clay, with rare laminations (Figure 7, section 47).

- **D55** is a 10 cm-thick with pebbles up to 2 cm in diameter.

342 **- U100 (Sedimentary unit 5)** displays highly bioturbated silty clay (Figure 9.6) and
343 rare silt/fine sand beds (Figure 6 and Figure7, section 61).
344 - **D50** is made of 2 coarse-grained intervals, about 50 cm-thick each, extremely rich
345 in biogenic material (Figure 9.7), separated by a bioturbated fine-grained interval,
346 with parallel laminations preserved in the sandy beds **(sedimentary unit 6)**.
347 Relatively high-diversity high-abundance molluscs assemblages are identified here
348 (Figure 10) with species pertaining to bivalves (*Myrtea spinifera*, *Nucula sp.*,
349 *Nuculana commutate*), scaphopods (*Dentalium*), and the typical prodeltaic
350 association *Turritella communis- Ditrupa arietina* (serpulids polychaetes).
351 **- U80** is a coarsening-upward sequence consisting (from top to bottom) in well-
352 sorted fine to very fine sand (see grain size and Gamma ray in Figure 6) with planar-
353 and cross-bedding **(sedimentary unit 7)** passing to mud-sand alternations with
354 intense bioturbation and occasional horizontal laminations (**sedimentary unit 8;**
355 Figure 8, sections 88, 90, 91).
356 - **D45** is a 25 cm-thick interval of medium sand with abundant shell debris
357 (**sedimentary unit 9;** Figure 9.9). Here, molluscs as *D. arietina* and *T. communis* are
358 associated with the solitary coral *Caryophyllia* and a number of bivalves e.g.
359 Veneridae species, *Dosinia lupinus*, *Saccella commutata*, *Parvicardium* sp, *Mytilus*
360 sp., etc.
361 **- U57** and **U40** includes clayey silts (**sedimentary units 10 and 13)** and
362 sandy/gravely deposits **(sedimentary units 11 and 12).**
363 **U40** consists of clayey silts with a very coarse interval (large rounded clasts and shell
364 fragments) at the bottom of the borehole (**sedimentary unit 14**; Figure 11C, Figure
365 9.10) in a muddy sand matrix (Figure 8, section 114; Figure 9.10). Penetrometer cone
366 resistance (*qt*, Figure 5) is widely used in this part of the borehole for lithological
367 prediction because of poor recovery. It allowed us to distinguish slight lithological
368 differences (medium to coarse sand).
369 A high degree of reworking concerns the bioclasts (worn and chalky fragments),
370 despite their abundance and diversity (Figure 10).
371
372 **4.3. Chrono- and biostratigraphic constraints**
373 **1) ^{14}C dates**
374 Radiocarbon dating has been carried out for the first 42 m of the borehole that fall
375 within the radiocarbon dating resolution (Table 2, Auxiliary Material).

We obtained good results for the top of the borehole (U155) and for the fine-grained interval of seismic U151 (Figure 12), whereas significant age inversions affect the sandy interval of U152 (Figure 12). Within the ^{14}C ages that are clearly distorted because of the occurrence of reworked material, it is worth noting that the measured ages show an overall trend from older (about 36 cal ky BP) to younger (26 cal ky BP) moving from the top to the bottom of the interval. Thus, rather than discarding them, we can use these data for discussing the nature of erosion during falling sea-levels and eventually, the origin of sediments deposits during forced regression (see **Discussion**).

2) Calcareous nannoplancton

Coccolithophore assemblages observed in the studied samples of PRGL2-2 are dominated by Noelaerhabdaceae. Reworked nannofossils are a common feature of all studied samples and are even present in the samples that are almost barren of calcareous nannoplancton. The age of basal sediments remains undetermined because of poor preservation of nannoplancton in sedimentary units 7 to 14. However, significant events are identified in the upper layers that allow a correlation with the oxygen isotope stack of *Lisiecki and Raymo* [2005], (Figure 12):

First Occurrence of *Emiliania huxleyi* is identified at 60.56 mbsf. The age of this event was established by *Thierstein et al.* [1977] at 268 ky (top of MIS- 8). It has to be taken into account that this First Occurrence horizon (lower limit of the present-day Nannofossil Zone NN21 of *Martini* [1971], could have been influenced by the low coccolithophore abundances in the samples.

Age of the top of the hole: the coccolithophore assemblage compositions and the high abundances present in the uppermost interval indicate that this horizon is younger than the last glacial period (scarcity of *E. huxleyi* >4 µm).

Other events: Despite the low abundance of calcareous nannoplancton in most samples, the following horizons can be approximated (Figure 12):

(a) Reversal in *Gephyrocapsa caribbeanica*/*Gephyrocapsa oceanica* - small *Gephyrocapsa*: *G. caribbeanica* and *G. oceanica* decrease their abundances and small *Gephyrocapsa* becomes the dominant group at about 62.93 mbsf. This event has been dated by *Villanueva et al.* [2002] and *Flores et al.* [2003] between 260 and 245 ky (top of MIS 8).

(b) Reversal in small *Gephyrocapsa–Gephyrocapsa muellerae*: This last species increases in abundance around 43.73 mbsf. This probably approximates the event occurring during the middle of MIS 6 (between 160-170 ky, as idenfied by *Villanueva et al*. [2002].

(c) Acme of *Emiliania huxleyi*/Reversal in *Gephyrocapsa muellerae* - *Emiliania huxleyi*: The latter increases its abundance at about 41.34 mbsf, approximating the position of MIS 4.

5. Discussion

Integration of geophysical multi-proxy borehole data allows us to propose a synthetic interpretation of Quaternary depositional units and surfaces in the Gulf of Lions (Table 1, Auxiliary Material).

5.1. Nature and origin of major erosion surfaces

A striking feature along PRGL2-2 is the perfect match between major seismic reflections (including the sea-floor) and very coarse intervals with shells and shell debris. The deposits with the richest mollusc content are associated with the major discontinuities. The mollusc assemblages are indicative of diverse environments, from open shelf to sub-littoral and are suggestive of an intense reworking. Cold-water Pleistocene species are found within D60, D50, D45 and D30 and described within D70 based on shallow cores [*Bassetti et al*., 2006].

The boreo-celtic guests have an important eco-biostratigraphic and climatic significance: *Modiolus modiolus*, *Arctica islandica*, cf. *Mya truncata/Panopea norvegica* known to proliferate in the Mediterranean only during glacial periods [*Malatesta and Zarlenga*, 1986]. They occur consistently in association with major bounding surfaces. Interestingly, these cold-water species are in most cases mixed with temperate species. The borehole data confirm previous seismic and sequence stratigraphic interpretations that the major seismic discontinuities are polygenetic erosion surfaces formed as sequence boundaries at the top of prograding wedges, during sea-level falls driven by 100 ky glacio-eustatic cycles, and subsequently reworked by marine ravinement during sea-level rises (see summaries *in Berné et al*. [2004]; *Rabineau et al.* [2005]). The age of ca.15 ky BP at the bottom of D70 found here (Figure 12) is consistent with ages given by *Bassetti et al.* [2006] and confirms that D70 was reworked by marine ravinement during the deglacial sea-level rise.

Transgressive deposits, which are very thin or absent on the outer shelf, except at the position of sand ridges (U155 in Figure 3) are capped by condensed surfaces during highstands. This observation explains the significant mix of glacial and "warm" fauna living at different water depths. In details, sediments corresponding to seismic surfaces D60, D50 and D45 include in all cases 2 coarse-grained intervals, separated by 10 cm to 1 m of very fine sand or silty clay material. These fine-grained intervals might correspond to transgressive deposits separating a *ravinement* surface (at the base) and a condensed interval (maximum flooding surface, at the top), as described for D70 by *Bassetti et al.* [2006]. The reduced thickness (<1m) of these transgressive deposits hampers their detection on seismic profiles.

The lowermost bounding surface (D30) falls in a distinctive lithologic interval, with a coarse-grained basal unit (sedimentary unit 14) including material such as rounded pebbles implying the vicinity of a river. On seismic profiles, these deposits correspond to the infill of an axial incision within the Bourcart canyon. This supports the idea of a genetic link between axial incisions that downcut canyon heads and rivers during lowstands, as proposed by *Baztan et al.* [2005].

5.2. General stratigraphic organization

Biostratigraphy allows us to propose a general chrono- and sequence stratigraphic interpretation of the study area. Major seismic units with steep clinoforms correspond to sandy shorefaces or delta fronts/prodeltas formed during major sea-level falls and ensuing lowstands of each 100 ky glacial cycles. The age of seismic unit U100 (MIS 6-7) is consistent with a MIS 8 origin for seismic U80, immediately beneath. The perfect preservation of U80 (including preservation of the topsets of the clinoforms) can be explained by substantial accommodation space formed by erosion during the two previous low stands of the sea (MIS 10 and MIS 12), that were much more pronounced than MIS 8. Within MIS 6, three major sub-units with thick (>20m) and steep (>3°) clinoforms, labelled U95, U110 and U130, have been previously identified and mapped in 3 dimensions (*Rabineau et al.*, [2005]; their Figures 7 and 8). Among these units, only U95 extends to the vicinity of the borehole (Figure 3), the others being situated in a more offshore and further east (*ibid*). In the absence of precise chrono-stratigraphic constraints, the origin of these multiple sand

bodies within one single 100-ky falling stage systems tract could be attributed to purely autocyclic processes, such as switching of deltaic lobes in a supply-dominated environment, with stable sea-level being. However, considering that there is at least a difference of 30 m in the depths of the topsets of clinoforms of units U95 and U130 (*ibid*), it is more reasonable to invoke an allocyclic (sea-level fall) origin. In this view, the lowstands corresponding to MIS 6.6, MIS 6.4 and MIS 6.2 could be good candidates for the formation of U95, U110 and U130, respectively.

5.3. Nature and significance of large clinoforms of U151/U152

The full recovery of sediments from seismic unit U151/U152, as well as the availability of precise time constraints (from absolute ^{14}C dates) for this interval allows discussion of the origin of large-scale clinoforms. These features have been often described from seismic data on many continental shelves, but rarely sampled. Comparison with similar features from ancient stratigraphic record adds another interest to our results.

1) Synthesis of sedimentological and biostratigraphic information on U151/U152

The sedimentary facies association within U151/U152 represents a typical coarsening upwards trend commonly described on wave-dominated shelves [*Walker and Plint*, 1992], with the vertical superposition of 3 main facies (from top to bottom):

1. planar to very low-angle stratified sand and possibly swaley cross-stratification (Figure 7, sedimentary unit 1, section 8A), indicative of efficient wave reworking. This deposit lies above an intensely bioturbated unit (Figure 7, sedimentary unit 1, section 10A);
2. cross stratified, well-sorted fine sands with parallel to low-angle converging laminations suggesting a possible hummocky cross-stratification (Figure 7, sedimentary unit 1, section 14A). The HCS unit represents deposition above storm but probably not far from wave base [*Dumas and Arnott*, 2006];
3. bioturbated mud with interbedded thin sand beds (Figure 7, sedimentary unit 2, sections 35 and 39). Storm-generated event beds, intensively bioturbated with sharp erosional base, corresponding to moderate-energy storm-dominated shelf zone with fair weather mud drapes [*Aigner and Reineck*, 1982].

The mutual stratigraphic position of these facies strongly supports the interpretation of U151/U152 as a regressive complex including foreshore and shoreface (and/or delta front/prodelta) domains. Sedimentary unit 1 is characterized by a high-energy (coastal) setting marked essentially by: (a) massive, well-sorted fine to medium sand with low carbonate content; (b) horizontal lamination and possible swaley cross stratification, indicative of winnowing by wave action; (c) possible hummocky cross-stratification indicative of a storm-dominated lower shoreface environment.

Storm beds are preferably recorded in the “offshore” facies (bottomsets, sedimentary unit 2) as testified by highly heterolithic deposits, mainly consisting of fine-grained beds alternating with repeated, distally deposited, storm beds. Bioturbation of the finer section (silty clay) indicates prolonged intervals of calm conditions between the deposition of tempestites. It has been argued that the so-called “offshore muds” do not really exist, and are in fact part of the lower shoreface domain because mud is trapped along shore by shelf circulation [*Dalrymple and Cummings*, 2005]. This is exactly what is observed in the Gulf of Lions, where mud is confined on the inner shelf [*Berne et al.*, 2007]. We therefore consider sedimentary unit 2 as part of the lower shoreface/prodelta domains.

2) Integration of sedimentological and seismic data

The upper 20 m massive sands of sedimentary unit 1 correspond to the steep (up to 5°) foresets of seismic unit U152. They pass progressively to sands with thin muddy interbeds between 20 and 30 mbsf where clinoforms are dipping more gently. The abrupt deepening of sedimentary facies below 30 mbsf corresponds to seismic surface D65. The alternating bioturbated sands and muds observed below this surface (sedimentary unit 2) correspond to the bottomsets of clinoforms of unit U151. Despite the dominant sandy lithology of clinoforms, the impedance contrast that is at the origin of reflectors on seismic profiles (foresets of U152) is likely due to the presence of cm-thick clayey layers, or packets of such layers.

Sedimentary structures and paleo-environmental indications given by fauna and micro-fauna confirm earlier interpretations, based on seismic stratal architectures (*Aloïsi* [1986] and subsequent workers): U151 and U152 represent wave-dominated shorefaces deposited during an overall sea-level fall at the end of the last glacial cycle.

The shoreface deposits observed here differ from typical shoreface modern deposits (highstand), which commonly show much gentler angle of clinoforms (0.3° on average, [*Walker and Plint* 1992], about 0.5° on the modern Sète shoreface [*Barusseau et al.*, 1994]). On the other hand, examples of clinoforms with steep dip angles are reported in the stratigraphic record in forced regressive shelf-margins [*Hanken et al.*, 1996; *Hart and Long*, 1996; *Massari et al.*, 1999; *Surlyk and Noe-Nygaard*, 2005]. Quaternary margins worldwide also document examples of sandy (or supposedly sandy) shelf or shelf-edge shoreface or deltaic clinoforms with angles of dip similar to that of the Gulf of Lions' shorefaces [*Anderson et al.*, 2004; *Chiocci and Orlando*, 1996; *Hernandez-Molina et al.*, 1994; *Hiscott*, 2001; *Suter and Berryhill*, 1985; *Sydow et al.*, 1992; *Trincardi and Field*, 1991; *Trincardi and Correggiari*, 2000; *Winn et al.*, 1998]. Possibly, the difference in slope angles between present-day shorefaces and Pleistocene/Ancient indicates that the latest record progradation with more abundant sand supply, whereas modern examples correspond to equilibrium profiles of sand-starved shorelines-shelf system. An alternative (or additional) explanation is that these shorefaces could in fact correspond to the "asymmetric wave-dominated deltas" that form updrift of deltaic systems subject to longshore drift [*Bhattacharya and Giosan*, 2003]. Such an asymmetry has been described on the modern Po delta [*Correggiari et al.*, 2005]. The steep dip angle of the clinoforms measured on seismic profiles is consistent with slope measured on the modern delta front of the active Roustan distributary channel of the Rhone, i.e. about 4° [*Maillet et al.*, 2006]. Another alternative explanation has been proposed by Trincardi (Pers. Comm.), these sand bodies being interpreted as the product of along-shore sediment advection to deeper areas of increased accommodation, as documented for the muddy regressive deposits on the Adriatic [*Cattaneo et al.*, 2007].

The thickness of the Gulf of Lions' shoreface deposits is also quite different from values reported from modern examples. It reaches up to 30 m for U152 (including 20 m of massive sands), and even 40 m for U80 (where sand thickness is estimated to be more than 30 m). These values have to be compared to the thickness of Holocene shorefaces, which are in the range of 10-20 m [*Hampson and Storms*, 2003]. On the other hand, they are comparable to the thickness of some ancient shoreface deposits such as the Kenilworth Member of the Book Cliffs [*Pattison and Walker*, 1995]. An explanation for this difference is that modern shorefaces prograde over inner shelves

where accommodation is limited because of the low gradient, whereas the shorefaces studied here developed at the shelf edge. In addition, the steep clinoforms of U151/152 and U80 developed immediately seaward of a step in the underlying surface (Figure 2). Probably this step provided additional accommodation for shoreface deposition, as proposed by *Trincardi and Field* [1991] for Tyrrhenian Sea shorefaces, or as observed at the outcrop scale by *Massari et al.* [1999].

In addition to this morphological control, *Hampson and Storms* [2003] proposed that the main processes (or recurrence of processes) controlling the architecture of modern and ancient shorefaces are substantially different: modern shorefaces represent a much shorter time-span, and therefore are mainly controlled by wave climate and/or sediment supply; in contrast, shorefaces from the geological record a shoreline trajectory [*Helland-Hansen and Martinsen*, 1996] during changing rate of relative sea-level rise. This could account both for the greater thickness of ancient shorefaces and for differences in clinoform dip angles. The available chrono-stratigraphic framework allows us to sustain this hypothesis.

5.4. Regressive downward stepping parasequences linked to pulsed sea-level falls

U151 and U152 were deposited during the overall sea-level fall that took place between the highest sea-level of Marine Isotope Stage (MIS) 3 (around 50 ky BP) and the lowest sea-level of MIS 2 (Last Glacial Maximum), around 22 cal ky BP. Even if the position of global sea-level during MIS 3 is still debated (ranging from -35 m to -95 m, see compilation of sea-level curves in *Jouet et al*., [2006], the MIS 3-MIS 2 interval record a period of overall cooling trend accompanied by lowering of sea-level, punctuated by rapid climate changes generally referred to as Dansgaard Oeschger (D/O) cycles [*Bond et al.*, 1993; *Dansgaard et al.*, 1993], with Heinrich Events (HE, *Heinrich* [1988]) occurring at the end of some of the coldest stadials.

In the lithological succession within U152/U151, we observed coarsening upward units indicative of a general regressive pattern that appear separated by flooding surfaces mantled by fine-grained sediment. In particular, such flooding surfaces are observed at about 29 and 40 mbsf which correspond to seismic reflections D64 and D65, and are indicated by sedimentary facies suggesting a relatively abrupt deepening as marked in Figure 13.

The chrono-stratigraphic constraints obtained from shallow cores (~20 m long) retrieved landward and seaward of PRGL2-2 [*Jouet et al.*, 2006], as well as the ^{14}C dates obtained within U151/152 at PRGL2-2 imply that:

- D65 formed between 24.13 and 22.7 cal ky BP (from *Jouet et al.* [2006]) a time frame consistent with an age <25 cal ky BP found at 33.75 mbsf on PRGL2-2, about 4 m below the position of D65 (considering an average sedimentation rate of 1 m/ky),
- D64 formed between 30.4 and 27.75 cal ky BP (if we assign a depth of about 40 mbsf for D64 at the position of this borehole).

Finally, the ages of both surfaces fall within the time-intervals assigned to HE 2 and HE 3 (respectively ~ 24 and 30 ky cal BP, *Hemming* [2004]). They also correspond to the end of marked periods of sea-level falls (in the order of 10 m) observed in the Red Sea [*Arz et al.*, 2007; *Siddall et al.*, 2003].

On seismic profiles, a very pronounced downward shift surface corresponds to seismic surface D63, that marks a very distinct erosional boundary between bottomsets of U147 and steep (probably sandy) clinoforms of U151 (Figure 13). At the resolution of seismic data, this surface is merged with the main sequence boundary (D60), however, we notice a distinctive fine-grained interval separating two very coarse intervals interpreted as *ravinement* surfaces. This interval has not been dated on PRGL2-2. However, it was dated previously in a piston core at ~ 41 cal ky BP [*Jouet et al.*, 2006], whereas an age of ~ 38 cal ky BP is found at the deep borehole PRGL1-4. The relevance of the erosion linked to D63, as it is seen on seismic profiles, can be explained by a much higher magnitude of sea-level drop between 43 and 40 ky cal BP (about 30 m according to *Arz et al*. [2007]). According to these authors, the magnitude of the ensuing sea-level rise was in the same order (Figure 13), within only ~2 ky (about 1.5 cm/y), i.e. a rate in the same range as that of melt water pulses during the last deglacial. The stratigraphic expression of this rapid transgressive interval could be the thin silt and clay layer situated at 41.51-41.56 mbsf between two coarse-grained intervals (Figure 11B), immediately above D60.

Finally, within the prograding shoreface deposits recording the overall sea-level fall between MIS 3 and MIS 2 display a sedimentary *motif* linked to higher-order incremental sea-level falls and subsequent rises (Figure 13) that erode the upper and

seaward terminations of previous deposits and initiate a new phase of forced regression. These minor bounding surfaces, created by these pulsations are genetically similar to the major bounding surfaces, in the sense that they represent surfaces linked both to a fall and rise of sea-level, but their lithologic expression is different from that of major bounding surfaces (D60, D50, D45, D30) because the magnitude of sea-level changes and duration of processes at their origin are shorter. This scenario also allows the explanation of the age inversion observed within the ^{14}C data from U152. In the context of general sea-level fall, the uppermost clinoform samples are sourced from deposits reworked from the entire emerged shelf (and therefore older on average). On the other hand, the deepest clinoforms correspond to a period of higher sea-level, and include less reworked material.

Our scenario of shoreface preservation in response to pulsed sea-level falls is quite similar to that proposed from the interpretation of ancient shoreface deposits. The concept was initially proposed by *Plint* [1988] and subsequently developed and applied to several ancient examples [*Hunt and Tucker*, 1992; *Mellere and Steel*, 2000; *Posamentier and Allen*, 1993; *Walker and Plint*, 1992]. A synthesis of the stratigraphic expression of such *"falling stage systems tracts"* is given by *Plint and Nummedal* [2000]. In the rock record, good examples of downstepping clinoform units separated by *ravinement* surfaces, very similar to our Gulf of Lions shoreface deposits, are given for instance by *Surlyk and Noe-Nygaard* [2005] from the lowermost Cretaceous of East Greenland. In modern (late Holocene) shoreface deposits, the effect of rapid, even if limited, sea-level falls (<1 m, in this case in relation with tectonic uplift) is well documented by *Tamura et al.* [2007] who show intra-shoreface erosion following tectonically-induced sea-level falls. Such surfaces are also reproduced by numerical experiments through sea-level fall and/or increase of the wave-height [*Storms and Hampson*, 2005]. The thickness of our shelf-edge shorefaces (compared to most of modern examples) could be ascribed to increased space available at the shelf edge, simply for geomorphologic reasons, or to intense erosion during part of MIS 3.

6. Summary and conclusions

1. The prograding bodies in the Gulf of Lions are formed by massive sand with clinoforms dipping at 5° maximum and showing a progressive transition to

silt to silty clay deposits basinwards that form coarsening-upward sedimentary sequences. The sedimentological *motif* of these deposits is summarized in Figure 13.

2. Theses sand bodies formed during the overall sea-level falls of the 100-ky glacial-interglacial cycles.
3. They are are bounded by easily recognizable erosional surfaces that display a common sedimentological expression (coarse grained material, shell and shell hash with species indicative of a variety of marine environments). Macrofauna (molluscs, corals) together with the lithological characteristics prove that these surfaces have a polygenetic origin (marine regressive erosion, subaerial erosion, marine transgressive ravinement and possible condensation during highstands). These surfaces form the ***major bounding surfaces*** recording 100-ky glacial-interglacial cycles. In several cases, mud deposits, 0.1 to 1 m thick are intercalated in these coarse beds and might represent transgressive deposits, not detected on seismic profiles.
4. Due to the composite shape of the sea-level curve, higher-frequency climatic cyles (20 and 40 ky) are also preserved in the form of prograding shoreface wedges. This is probably the case for MIS 6.2, 6.4 and 6.6.
5. Our results differ from those of the Adriatic sites of PROMESS [*Ridente et al.*, in press] where shelf deposits are mainly composed of prograding interglacial fine-grained deposits, due to increased southward advection of sediments from the Po during high stands of sea-level.
6. Within the last glacial/interglacial sequence, cyclic changes of sedimentary environments show that the clinostratified bodies are composed of several higher-order (para)sequences, bounded by flooding surfaces. Radiocarbon dates indicates that these ***minor bounding surfaces*** record rapid sea-level changes during the overall MIS3-MIS2 sea-level fall, in phase with the high-resolution isotopic records of the Red Sea [*Arz et al.*, 2007; *Siddall et al.*, 2003].
7. Each parasequence (about 40 m thick, including about 20 m of massive sand) formed within about 5-10 ky, and progradation during this interval was in the range of 1-2 km. The sea-level drops that triggered progradation were of the order of 10-30 m.

8. The detection of river-derived material at the bottom of the borehole (unit 14), testifies the direct influence of fluvial discharge events at the shelf edge. This is the first evidence in this area of a connection between a lowstand river drainage and a canyon.

718

Acknowledgements

719 The drilling operation was conducted within the European project PROMESS 1
720 (contract EVR1-CT–2002-40024). Data were processed and interpreted with the
721 support of the French Agence Nationale de la Recherche (ANR, contract NT05-3-
722 42040). Initial support for seismic data acquisition was provided by Ifremer, the French
723 “Margins” program, and the EC-funded «Eurostrataform project (contract EVK3-2001-
724 00200). Engineers of FUGRO-BV and the captain and crew of the Amige drilling
725 vessel «Bavenit» are warmly thanked for their dedication during the cruise.
726 The European Promess shipboard party (http://www.pangaea.de/Projects/PROMESS1)
727 and colleagues at Ifremer (A.S. Alix, F. Duval, G. Ph. Fernagu, G. Floch, N. Frumholtz,
728 B. Marsset, L. Morvan, D. Pierre, M. Rovere, E. Thereau, Y. Thomas) are also thanked
729 for various contributions during all phases of data acquisition and processing.
730 A. Ceregato (University of Bologna) is thanked for revising the mollusc taxonomy.
731 The authors of this paper are indebted to G-cubed Editors L.D. Labeyrie and V. Salters,
732 Associate Editor F. Trincardi, as well as to G.Plint and an anonymous reviewer, for
733 their thorough review of the manuscript.
734 This is a IGM contribution n. 1596.
735 The first author benefited from fellowships from «Eurostrataform» and ANR at
736 IFREMER (Centre de Brest).

738

739 **References**

740 Aigner, T., and H.-E. Reineck (1982), Proximality trends in modern storm sands from
741 the Helgoland Bight (North Sea) and their implication for basin analysis,
742 *Senckenbergiana Maritima*, *14*, 183-215.
743 Aloïsi, J. C. (1986), Sur un modèle de sédimentation deltaïque: contribution à la
744 connaissance des marges passives, *Unpublished Doctoral Thesis, University of*
745 *Perpignan, 162 p.*
746 Anderson, J. B., A. Rodriguez, K. C. Abdulah, R. H. Fillon, L. A. Banfield, H. A.
747 McKeown, and J. S. Wellner (2004), Late Quaternary Stratigraphic evolution of the
748 northern Gulf of Mexico margin: a synthesis, in *Late Quaternary Stratigraphic*
749 *evolution of the northern Gulf of Mexico margin*, edited by J. B. Anderson and R. H.
750 Fillon, pp. 1-23, SEPM (Society for Sedimentary Geology), Tulsa.
751 Arz, H. W., F. Lamy, A. Ganopolski, N. Nowaczyk, and J. Patzold (2007), Dominant
752 Northern Hemisphere climate control over millennial-scale glacial sea-level variability,
753 *Quaternary Science Reviews*, *26*(3-4), 312-321.
754 Austin, J. A., N. Christie-Blick, M. J. Malone, and e. al. (1998), *Proc. ODP, Init.*
755 *Repts., 174A*, Ocean Drilling Program, College Station, TX
756 Bard, E., M. Arnold, B. Hamelin, N. Tisnerat-Laborde, and G. Cabioch (1998),
757 Radiocarbon calibration by means of mass spectrometric 230Th/234U and 14C ages of
758 corals. An updated data base including samples from Barbados, Mururoa and Tahiti,
759 *Radiocarbon*, *40*(3), 1085-1092.
760 Barusseau, J. P., M. Radulescu, C. Descamps, C. Akouango, and A. Gerbe (1994),
761 Morphosedimentary multiyear changes on a barred coast (Gulf of Lions, Mediterranean
762 Sea, France), *Marine Geology*, *122*, 47-62.
763 Bassetti, M. A., G. Jouet, F. Dufois, S. Berne, M. Rabineau, and M. Taviani (2006),
764 Sand bodies at the shelf edge in the Gulf of Lions (Western Mediterranean): Deglacial
765 history and modern processes, *Marine Geology*, *234*, 93-109.
766 Baztan, J., S. Berne, J. L. Olivet, M. Rabineau, D. Aslanian, M. Gaudin, J. P. Rehault,
767 and M. Canals (2005), Axial incision: The key to understand submarine canyon
768 evolution (in the western Gulf of Lion), *Marine and Petroleum Geology*, *22*(6-7), 805-
769 826.
770 Berne, S., G. Jouet, M. A. Bassetti, B. Dennielou, and M. Taviani (2007), Late Glacial
771 to Preboreal sea-level rise recorded by the Rhone deltaic system (NW Mediterranean),
772 *Marine Geology*, *245*(1-4), 65-88.
773 Berné, S., G. Lericolais, T. Marsset, J. F. Bourillet, and M. de Batist (1998), Erosional
774 shelf sand ridges and lowstand shorefaces: examples from tide and wave dominated
775 environments of France, *Journal of Sedimentary Research*, *68*(4), 540-555.
776 Berné, S., M. Rabineau, J. A. Flores, and F. J. Sierro (2004), The impact of Quaternary
777 Global Changes on Strata Formation. Exploration of the shelf edge in the Northwest
778 Mediterranean Sea, *Oceanography*, *17*(4), 92-103.
779 Berné, S., and C. Gorini (2005), The Gulf of Lions: An overview of recent studies
780 within the French 'Margins' programme, *Marine and Petroleum Geology*, *22*(6-7), 691-
781 693.
782 Bhattacharya, J. P., and L. Giosan (2003), Wave-influenced deltas: geomorphological
783 implications for facies reconstruction, *Sedimentology*, *50*(1), 187-210.
784 Bond, G. C., W. Broecker, S. Johnsen, J. McManus, L. Labeyrie, J. Jouzel, and G.
785 Bonani (1993), Correlations between climate records from North Atlantic sediments
786 and Greenland ice, *Nature*, *365*(6442), 143-147.
787 Brookfield, M. E. (1977), The origin of bounding surfaces in ancient eolian sandstones,
788 *Sedimentology*, *24*, 303-332.

789 Cattaneo, A., F. Trincardi, A. Asioli, and A. Correggiari (2007), The Western Adriatic
790 shelf clinoform: energy-limited bottomset, *Continental Shelf Research*, *27*(3-4), 506-
791 525.
792 Chiocci, F. L., and L. Orlando (1996), Lowstand terraces on Tyrrhenian Sea steep
793 copntinental slopes, *Marine Geology*, *134*, 127-143.
794 Correggiari, A., A. Cattaneo, and F. Trincardi (2005), The modern Po Delta system:
795 Lobe switching and asymmetric prodelta growth, *Marine Geology*, *222-223*, 49-74.
796 Dalrymple, R. W., and D. I. Cummings (2005), The offshore transport of mud: why it
797 doesn't happen and the stratigraphic implications, paper presented at Geol. Soc.
798 America Annual Meeting, Abstracts with Programs.
799 Dansgaard, W., S. J. Johnsen, H. B. Clausen, N. S. Dahl-Jensen, C. U. Hammer, C. S.
800 Hvidberg, J. P. Steffensen, A. E. Sveinbjörnsdottir, J. Jouzel, and G. C. Bond (1993),
801 Evidence for general instability of past climate from a 250-kyr ice-core record, *Nature*,
802 *364*, 218-220.
803 Davis, R. A., and P. B. Balson (1992), Stratigraphy of a North Sea tidal sand ridge,
804 *Journal of Sedimentary Petrology*, *62*(1), 116-121.
805 Dumas, S., and R. W. C. Arnott (2006), Origin of hummocky and swaley cross-
806 stratification. The controlling influence of unidirectional current strength and
807 aggradation rate *Geology*, *34*(12), 10731076.
808 Flores, J.-A., M. Marino, F. J. Sierro, D. A. Hodell, and C. D. Charles (2003),
809 Calcareous plankton dissolution pattern and coccolithophore assemblages during the
810 last 600 kyr at ODP Site 1089 (Cape Basin, South Atlantic): paleoceanographic
811 implications, *Palaeogeography, Palaeoclimatology, Palaeoecology*, *196*(3-4), 409-426.
812 Hampson, G. J., and J. E. A. Storms (2003), Geomorphological and sequence
813 stratigraphic variability in wave-dominated, shoreface-shelf parasequences,
814 *Sedimentology*, *50*, 667-701.
815 Hanken, N.-M., R. G. Bromley, and J. Miller (1996), Plio-Pleistocene sedimentation in
816 coastal grabens, north-east Rhodes, Greece, *Geological Journal*, *31*(4), 393-418.
817 Harms, J. C., J. B. Southard, D. R. Spearing, and R. G. Walker (1975), *Depositional*
818 *environments as interpreted from primary sedimentary structures and stratification*
819 *sequences*, 161 pp., Tulsa.
820 Hart, B. S., and B. F. Long (1996), Forced regressions and lowstand deltas: Holocene
821 Canadian examples, *Journal of Sedimentary Research*, *66*(4), 820-829.
822 Helland-Hansen, W., and O. J. Martinsen (1996), Shoreline trajectories and sequences:
823 description of variable depositional-dip scenarios, *Journal of Sedimentary Research*,
824 *66*(4), 670-688.
825 Hendriks, P. H. G. M. (2003), In-depth gamma ray studies: borehole measurements,
826 Rijksuniversiteit Groningen, Holland.
827 Hernandez-Molina, F. J., L. Somoza, J. Rey, and L. Pomar (1994), Late Pleistocene-
828 Holocene sediments on the Spanish continental shelves: Model for very high resolution
829 sequence stratigraphy, *Marine Geology*, *120*, 129-174.
830 Hiscott, R. N. (2001), Depositional sequences controlled by high rates of sediment
831 supply, sea-level variations, and growth faulting: the Quaternary Baram Delta of
832 northwestern Borneo, *Marine Geology*, *175*(1-4), 67-102.
833 Hughen, K. A., and e. al. (2004), Marine04 Marine radiocarbon age calibration, 26 - 0
834 ka BP, *Radiocarbon*, *46*, 1059-1086.
835 Hunt, D., and M. E. Tucker (1992), Stranded parasequences and the forced regressive
836 wedge systems tract: deposition during base-level fall, *Sedimentary Geology*, *81*, 1-9.
837 Jouet, G., S. Berné, M. Rabineau, M. A. Bassetti, P. Bernier, and B. Dennielou (2006),
838 Shoreface migrations at the shelf edge and sea-level changes around the Last Glacial
839 Maximum (Gulf of Lions, NW Mediterranean Sea), *Marine Geology*, *234*(1-4), 21-42.

Leckie, D. A., and R. G. Walker (1982), Storm- and tide-dominated shorelines in Cretaceous Moosebar-Lower gates interval-outcrop equivalents of deep basin gas trap in western Canada, *American Association of Petroleum Geologists Bulletin*, *66*, 138-157.

Lee, H. J., J. P. M. Syvitski, G. Parker, D. Orange, J. Locat, E. W. H. Hutton, and J. Imran (2002), Distinguishing sediment waves from slope failure deposits: field examples, including the 'Humboldt slide', and modelling results, *Marine Geology*, *192*(1-3), 79-104.

Lisiecki, L. E., and M. E. Raymo (2005), A Pliocene-Pleistocene stack of 57 globally distributed benthic δ18O records *Paleoceanography*, *20*, PA1003.

Lobo, F. J., J. M. Dias, F. J. Hernandez-Molina, R. Gonzalez, L. M. Fernandez-Salas, and V. Diaz Del Rio (2005), Late Quaternary shelf-margin wedges and upper slope progradation in the Gulf of Cadiz margin (SW Iberian Peninsula), *Geological Society of London, Special Publications*, *244*, 7-25.

Lofi, J., M. Rabineau, C. Gorini, S. Berne, G. Clauzon, P. De Clarens, A. Tadeu Dos Reis, G. S. Mountain, W. B. F. Ryan, M. S. Steckler, and C. Fouchet (2003), Plio-Quaternary prograding clinoform wedges of the western Gulf of Lion continental margin (NW Mediterranean) after the Messinian Salinity Crisis, *Marine Geology*, *198*(3-4), 289-317.

Maillet, G. M., C. Vella, S. Berne, P. L. Friend, C. L. Amos, T. J. Fleury, and A. Normand (2006), Morphological changes and sedimentary processes induced by the December 2003 flood event at the present mouth of the Grand Rhone River (southern France), *Marine Geology*, *234*(1-4), 159-177.

Malatesta, A., and F. Zarlenga (1986), Northern guests in the Pleistocene Mediterranean Sea, *Geologica Romana*, *25*, 91-154.

Martini, E. (1971), Standard Tertiary and Quaternary calcareous nannoplankton zonation, paper presented at 2nd Planktonic Conference 1970, Edizioni Tecnoscienza, Rome.

Massari, F., M. Sgavetti, D. Rio, A. D'Alessandro, and G. Prosser (1999), Composite sedimentary record of falling stages of Pleistocene glacio-eustatic cycles in a shelf setting (Crotone basin, south Italy), *Sedimentary Geology*, *127*(1-2), 85-110.

Mellere, D., and R. J. Steel (2000), Style contrast between forced regressive and lowstand/transgressive wedges in the Campanian of south-central Wyoming (Hatfield Member of the Haystack Mountains Formation, in *Sedimentary responses to forced regressions*, edited by D. Hunt and R. Gawthorpe, pp. 141-162, Geological Society, Special Publications, London.

Monaco, A. (1971), Contribution à l'étude géologique et sédimentologique du plateau continental du Roussillon, Unpublished Doctor Thesis thesis, 295 pp, Perpignan, Perpignan.

Pattison, S. A. J., and R. G. Walker (1995), Sequence stratigraphic significance of sharp-based lowstand shoreface deposits, Kenilworth Member, Book Cliffs, Utah, *J. Sediment. Petrol.*, *79*(3), 444-462.

Plint, A. G. (1988), Sharp-based shoreface sequences and "offshore bars" in the Cardium Formation of Alberta: their relationship to relative changes in sea level, in *Sea-level changes: an integrated approach*, edited by C. K. Wilgus, et al., pp. 357-370, SEPM Special Publication No. 42, Tulsa.

Plint, A. G., and D. Nummedal (2000), The falling stage systems tract: recognition and importance in sequence stratigraphy, in *Sedimentary responses to forced regressions*, edited by D. Hunt and R. L. Gawthorpe, pp. 1-17, Geological Society, London.

Posamentier, H. W., G. P. Allen, D. P. James, and M. Tesson (1992), Forced regressions in a sequence stratigraphic framework: concepts, examples and exploration significance, *American Association of Petroleum Geologists Bulletin*, *76*, 1687-1709.

Posamentier, H. W., and G. P. Allen (1993), Variability of the sequence stratigraphic model: effects of local basin factors, *Sedimentary Geology*, *86*, 91-109.

Rabineau, M. (2001), Un modèle géométrique et stratigraphique des séquences de dépôt quaternaires sur la marge du Golfe du Lion : Enregistrement des cycles climatiques de 100000 ans, PhD thesis, 480 pp, University of Rennes 1, Rennes.

Rabineau, M., S. Berne, D. Aslanian, J.-L. Olivet, P. Joseph, F. Guillocheau, J.-F. Bourillet, E. Ledrezen, and D. Granjeon (2005), Sedimentary sequences in the Gulf of Lion: A record of 100,000 years climatic cycles, *Marine and Petroleum Geology*, *22*(6-7), 775-804.

Rabineau, M., S. Berne, J.-L. Olivet, D. Aslanian, F. Guillocheau, and P. Joseph (2006), Paleo sea levels reconsidered from direct observation of paleoshoreline position during Glacial Maxima (for the last 500,000[no-break space]yr), *Earth and Planetary Science Letters*, *252*(1-2), 119-137.

Raffi, I., and J. A. Flores (1995), Pleistocene through Miocene calcareous nannofossils from eastern equatorial Pacific Ocean (Leg 138), in *Proceedings of the Ocean Drilling Program. Scientific results* edited by N. G. Pisias, et al., pp. 233-286, Ocean Drilling Program, College Station.

Ramsey, N. (2002), *A calibrated model for the interpretation of cone penetration tests (CPTs) in North Sea quaternary soils*, London.

Reimer, P. J., M. G. L. Baillie, E. Bard, A. Bayliss, J. W. Beck, C. J. H. Bertrand, P. G. Blackwell, C. E. Buck, G. S. Burr, K. B. Cutler, P. E. Damon, R. L. Edwards, R. G. Fairbanks, M. Friedrich, T. P. Guilderson, A. G. Hogg, K. A. Hughen, B. Kromer, F. G. McCormac, S. W. Manning, C. B. Ramsey, R. W. Reimer, S. Remmele, J. R. Southon, M. Stuiver, S. Talamo, F. W. Taylor, J. van der Plicht, and C. E. Weyhenmeyer (2004), IntCal04 Terrestrial radiocarbon age calibration, *Radiocarbon*, *46*, 1029-1058.

Ridente, D., F. Trincardi, A. Piva, A. Asioli, and A. Cattaneo (in press), Sedimentary response to climate and sea level changes during the past ~400 kyr from borehole PRAD1-2 (Adriatic margin), *Geochemistry, Geophysics, Geosystems*.

Robertson, P. K. (1990), Soil classification using the cone penetration test, *Canadian Geotechnical Journal*, *27*(1), 151-158.

Siddall, M., E. J. Rohling, A. Almogi-Labin, C. Hemleben, D. Meischner, I. Schmelzer, and D. A. Smeed (2003), Sea-level fluctuations during the last glacial cycle, *Nature*, *423*, 853-858.

Stuiver, M., and P. J. Reimer (1993), Extended 14C database and revised CALIB radiocarbon calibration program, *Radiocarbon*, *35*, 215-230.

Surlyk, F., and N. Noe-Nygaard (2005), A forced-regressive shelf-margin wedge formed by transition-slope progradation: lowermost Cretaceous Rauk Plateau Member, Jameson Land, East Greenland *Bulletin of the Geological Society of Denmark*, *52*, 227-243.

Suter, J. R., and H. L. J. Berryhill (1985), Late Quaternary shelf-margin deltas, Northwest Gulf of Mexico, *Bull. Am. Assoc. Petrol. Geol.*, *69*(1), 77-91.

Sydow, J., H. H. Roberts, A. H. Bouma, and R. Winn (1992), Constructional subcomponents of a shelf-edge delta, Northeast Gulf of Mexico, paper presented at Transactions of the 42nd Annual Convention, GCAGS/GCS-SEPM, Jackson, Mississippi.

Tamura, T., F. Nanayama, Y. Saito, F. Murakami, R. E. I. Nakashima, and K. Watanabe (2007), Intra-shoreface erosion in response to rapid sea-level fall:

939 depositional record of a tectonically uplifted strand plain, Pacific coast of Japan,
940 *Sedimentology*, *54*(5), 1149-1162.
941 Tesson, M., B. Gensous, G. P. Allen, and C. Ravenne (1990), Late Quaternary lowstand
942 wedges on the Rhône Continental Shelf, France, *Marine Geology*, *91*, 325-332.
943 Tesson, M., H. W. Posamentier, and B. Gensous (2000), Stratigraphic organization of
944 Late Pleistocene deposits of the western part of the Rhone shelf (Languedoc shelf) from
945 high resolution seismic and core data, *AAPG Bulletin*, *84*(1), 119-150.
946 Thierstein, H. R., K. R. Geitznauer, B. Molfino, and N. J. Shackleton (1977), Global
947 synchroneity of late Quaternary coccolith datum levels: validation by oxygen isotopes,
948 *Geology*, *5*, 400-404.
949 Trincardi, F., and M. Field (1991), Geometry, lateral variability and preservation of
950 downlapped regressive shelf deposits: Eastern Tyrrhenian margin, Italy, *Journal of*
951 *Sedimentary Petrology*, *61*, 775-790.
952 Trincardi, F., and A. Correggiari (2000), Quaternary forced regression deposits in the
953 Adriatic Basin and the record of composite sea-level cycles, in *Sedimentary responses*
954 *to forced regressions*, edited by D. Hunt and R. L. Gawthorpe, pp. 245-269, Geological
955 Society, London.
956 van Wagoner, J. C., R. M. Mitchum, K. M. Campion, and V. D. Rahmanian (1990),
957 *Siliciclastic sequence stratigraphy in well logs, cores and outcrops*, 55 pp., American
958 Association of Petroleum Geologists.
959 Van Wagooner, J. C., R. M. Mitchum, K. M. Campion, and V. D. Rahamanian (1990),
960 Siliciclastic sequence stratigraphy in well logs, cores, and outcrops, *AAPG methods in*
961 *exploration series*, *7*, 55.
962 Villanueva, J., J. A. Flores, and J. O. Grimalt (2002), A detailed comparison of the
963 Uk'37 and coccolith records over the past 290 kyears: implications to the alkenone
964 paleotemperature method, *Organic Geochemistry*, *33*(8), 897-905.
965 Walker, R. G., and A. G. Plint (1992), Wave- and storm- dominated shallow marine
966 systems, in *Facies Models - Response to Sea Level Changes*, edited by R. G. Walker
967 and N. P. James, pp. 219-238, Geological Association of Canada, St John.
968 Winn, R. D., H. H. Roberts, B. Kohl, R. H. Fillon, A. Bouma, and R. E. Constans
969 (1995), Latest Quaternary deposition on the outer shelf, northern Gulf of Mexico; facies
970 and sequence stratigraphy from Main Pass Block 303 shallow core *Geological Society*
971 *of America Bullettin*, *107*(7), 851-866.
972 Winn, R. D., H. H. Roberts, B. Kohl, R. H. Fillo, J. A. Crux, A. H. Bouma, and H. W.
973 Spero (1998), Upper Quaternary strata of the upper continental slope, northeast Gulf of
974 Mexico: sequence stratigraphic model for a terrigeneous shelf edge, *Journal of*
975 *Sedimentary Research*, *68*(4), 579-595.
976
977
978 **Figure captions**
979
980 **Figure 1:** General bathymetry of the Gulf of Lions. The grey pattern
981 corresponds to the sand distribution on continental shelf. The red dotted line marks the
982 seaward termination of glacial sandy shorefaces.
983 **Figure 2**: Multi-channel, high-resolution sesmic profiles at the drill site: (A)
984 Shelf-slope seismic line (Marion 12) showing depositional sequences bounded by

discontinuities on the shelf that can be followed into correlative conformities on the slope (PRGL1-4 site); (B) close-up view at the position of PRG2-2 (line Calimero8).

Figure 3: High resolution multi-channel (A) and very high-resolution (sparker) (B) seismic profiles showing the detail on the last sequence (bounded by D60 and D70 discontinuities). See position in Figures 1 and 2. Post-glacial transgressive deposits (U155) lie above the clinostratified sequence. C.S. = cemented sand.

Figure 4: Correlation between seismic and lithological data after the conversion of mbsf depths into mstwtt on the basis of P-wave velocities from MSCL. Sedimentary units 1-14 are detailed in Table 1 (Auxiliary Material).

Figure 5: Geotechnical and physical properties measured at PRGL2-2 site. Lithological characteristics and soil types show an outstanding correspondence that can be used for lithological prediction of non-recovered intervals. The main lithologies are estimated by the combination of resistance to cone penetration (*qt*) and friction resistance (*fs*) for sediments comprised between clay and medium sand. Thick coarse grained horizons are not evidenced by this methodology. Between 2 and 5.5 mbsf the lack of pore pressure measurements (due to the high permeability of sand) does not allow lithological properties to be established. In addition, slight discrepancies between lithological prediction and real lithology are observed (see transition between sedimentary units 1-2 and 6-7). In fact, the CPTU has been measured 3 m away from PRGL2-2 and lateral facies changes might be possible.

Figure 6: Total sand fraction, carbonate content and and natural gamma ray counts at PRGL2-2 and correlation with corresponding sedimentary units. Note that the grain size analysis only takes into account the <2 mm fraction, therefore gravel and shell beds are not shown in the vertical profile.

Figure 7: X-ray images (see position in depth in Figures 4 and 6) evidencing sedimentary facies and structures: horizontal lamination and swaley cross bedding (8A), bioturbated sand (10A), hummocks and associated parallel lamination (14A), bioturbated storms beds in mud (35, 39), bioturbated clays with rare laminated silty beds (40, 47 and 61)

Figure 8: X-ray images (see position in depth in Figures 4 and 6) evidencing sedimentary facies and structures: intensively bioturbated clays with laminated sand beds (81), heterolithic facies (90 and 91 comparable to 35 and 39 in Figure 7), muddy shelly lag deposits with associated silty-sand bioturbated layers (103), alternating sand and mud couplets, slightly bioturbated (111), bioclastic material lag (worm tubes can be

distinguished) with bioturbated clay passing upwards to horizontally laminated silty clay (113), sand/clay alternations with sparse biogenic material (114)

Figure 9 : Photos from selected cores:

1- section 8B/37-57 cm (8.50-8.70 mbsf): mud intervals in massive sands;

2- section 32/2-22 cm (32.61-32.80 mbsf): silty clay with fine sand beds, large burrow;

3- section 34/23-43 cm (34.43-34.63 mbsf): Lenticular/wavy fine sand/silt beds and clay. Erosional basal contacts;

4- section 36/25-45 cm (36.05-36.25 mbsf): lenticular (rippled?) fine sand beds and clay/silty clay. Some scours at the bottom of sand beds;

5- section 40/30-50 cm (39.30-39.50 mbsf): Intensely bioturbated silty clay with organic matter spots;

6- section 69/1-21 cm (62.21-62.40 mbsf): very bioturbated clay/silty clay;

7- section 74/20-40 cm (66.40-66.60 mbsf): muddy bioclastic gravel;

8- section 91/30-50 cm(80.94-81.10 mbsf): graded silty sand beds in silty clay;

9- section 95/0-20 cm (83.60-83.80 mbsf): very coarse-coarse muddy sand with very abundant shells and shell fragments, including complete bivalves;

10- section 116/64-84 cm (99.57-100.13 mbsf): Sandy gravel with large rounded clasts (up to 3cm)

Figure 10: Synthetic scheme of mollusc assemblages examined in correspondence of erosion surfaces.

Figure 11: Detailed logs of selected cores. (A) Part of a sub-unit of sedimentary unit 2 showing an overall coarsening upward pattern with storm-generated beds based by an interval of clay, intensively bioturbated and with an high content of organic matter; (B) Coarse grained interval of the sedimentary unit 3 (corresponding to seismic surface D60), consisting of 2 coarse-grained beds (with shells and heterogeneous biogenic material) separated by about 1 m of marine clays; (C) the fining upward basal coarse-grained interval (sedimentary unit 14) made of sand and gravel (channel infill deposits)

Figure 12: Chronostratigraphy of PRGL2-2 and correlation with the sea-level curve [*Lisiecki and Raymo*, 2005]. ^{14}C dates provide an accurate chronology of the last sequence (U151-152). Deeper in the borehole, the detection of significant nannoplacton events are utilized down to MIS 8. The bottom of the hole has been dated on the basis of seismic correlations with the PRGL1-4 borehole (see Figure 2).

Figure 13 : Synthetic interpretation of the last forced-regressived unit (last 100 ky glacial-intergacial cycle between D60 and the sea-floor) showing the stratigraphic signature of higher-order, stepped sea-level falls creating 2nd order bounding surfaces (D63, D64, D65). Note the good match between the ages of these surfaces and the Heinrich events 4, 3, 2, respectively. D63, in particular, shows a drastic shallowing of sedimentary facies that could be explained by the 30m sea-level fall measure by *Arz et al*. [2007] in Red Sea. For clarity, post LGM deposits (U155) have not been represented.

Auxiliary material

Appendix A: Mollusc fauna components

Appendix B: Stratigraphical distribution of Gasteropoda and Bivalvia in PRGL2-2

Appendix C: Sedimentary unit descriptions, geotechnical properties, grain size, carbonate content and gamma-ray counts

Table1 : Definition of sedimentary units in PRGL2-2

Table 2 : ^{14}C dates in PRGL2-2

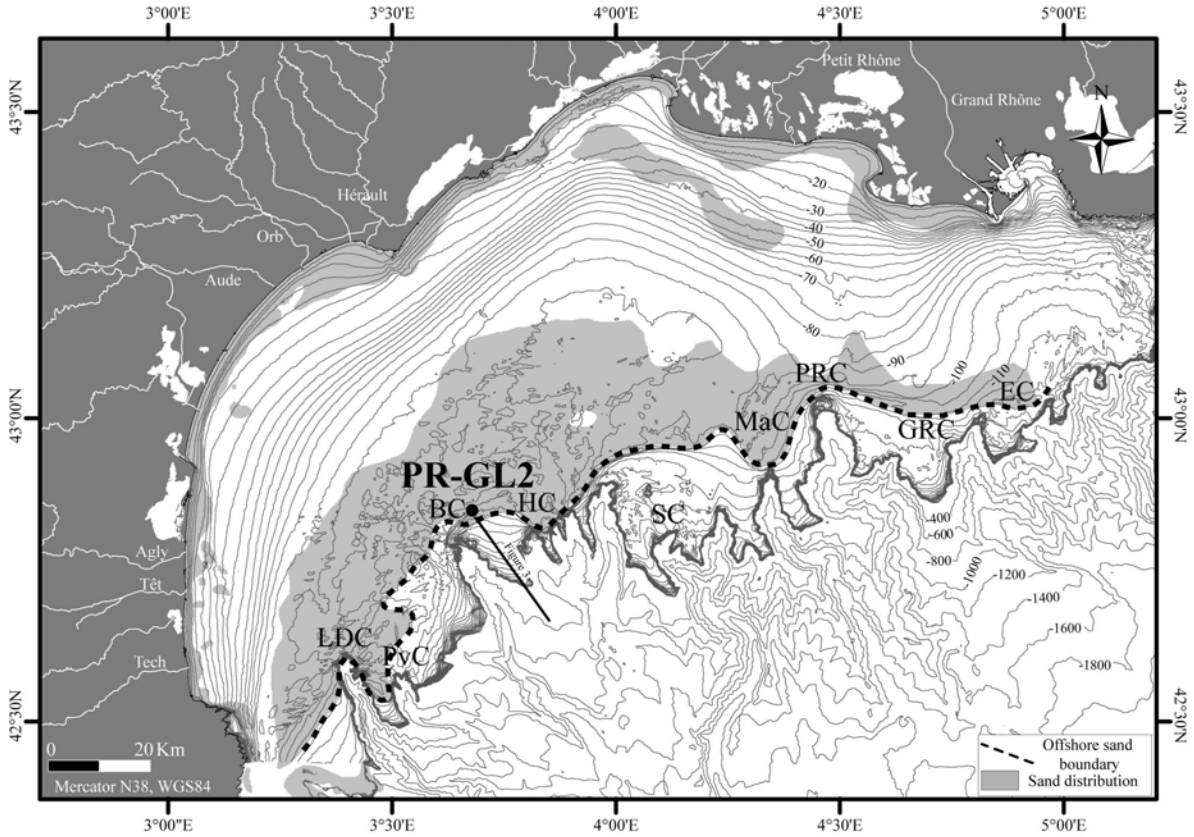

Figure1_Bassetti et al._G3

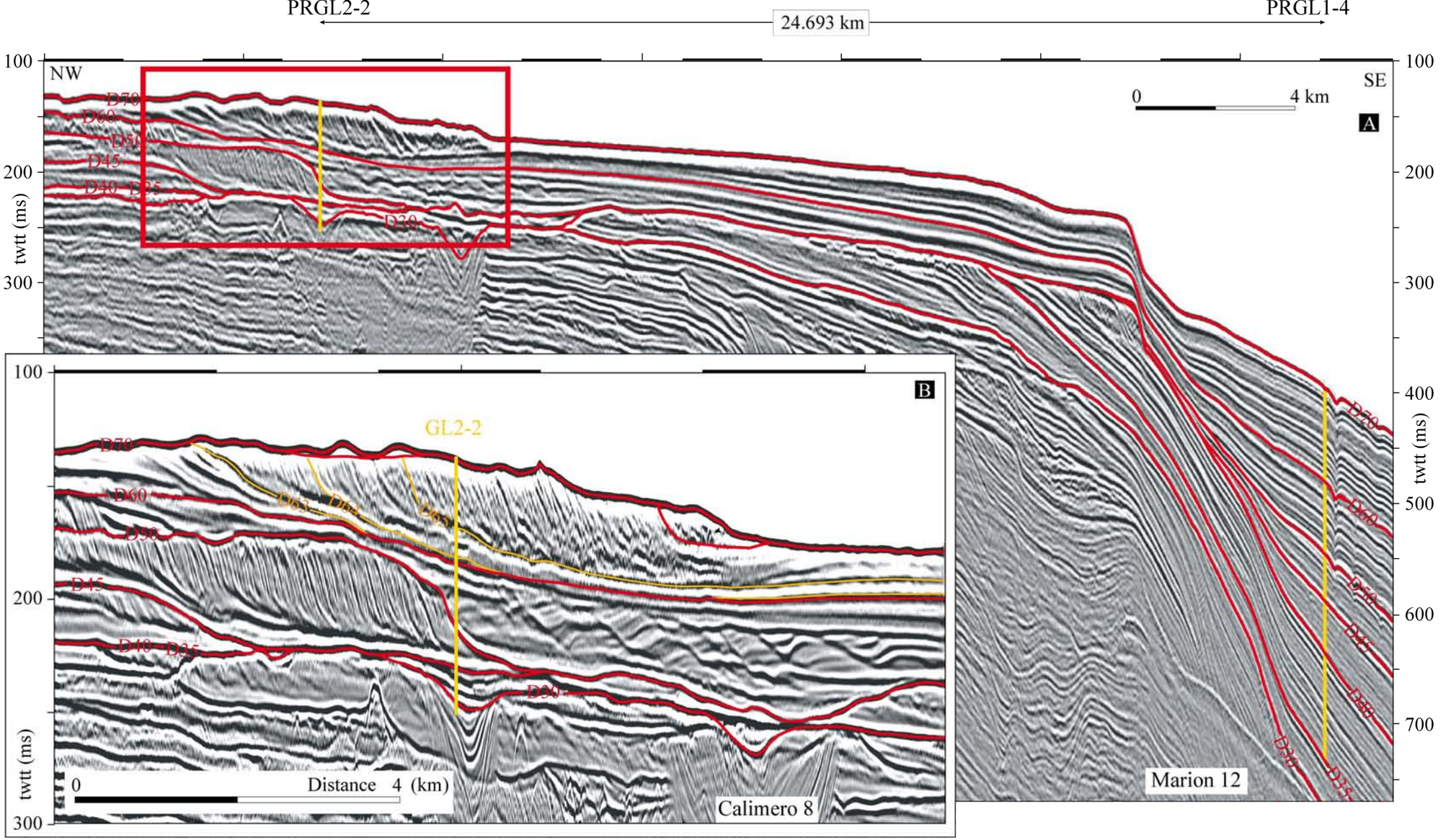

Figure 2_Bassetti et al._G3

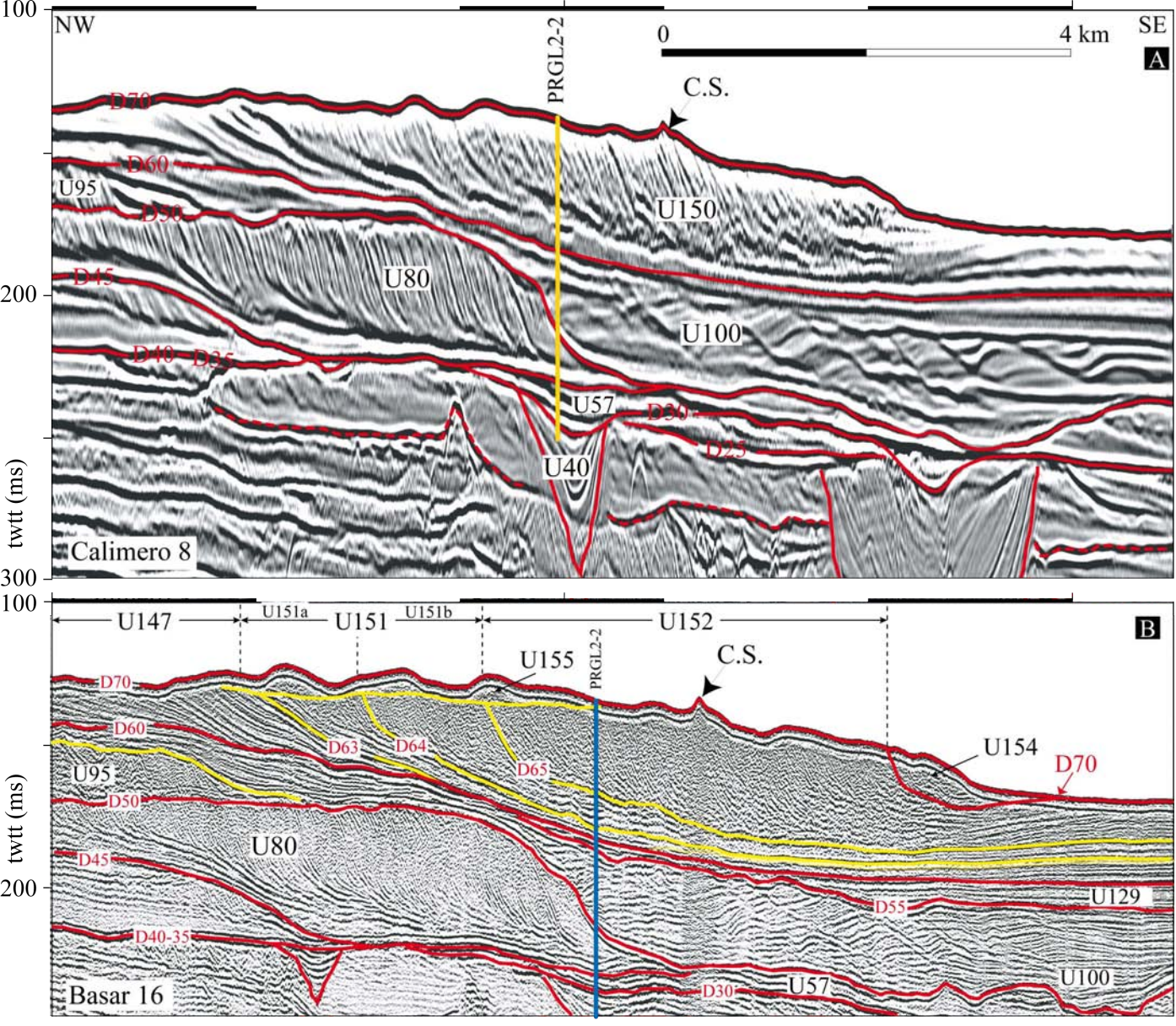

Figure 3_Bassetti et al._G3

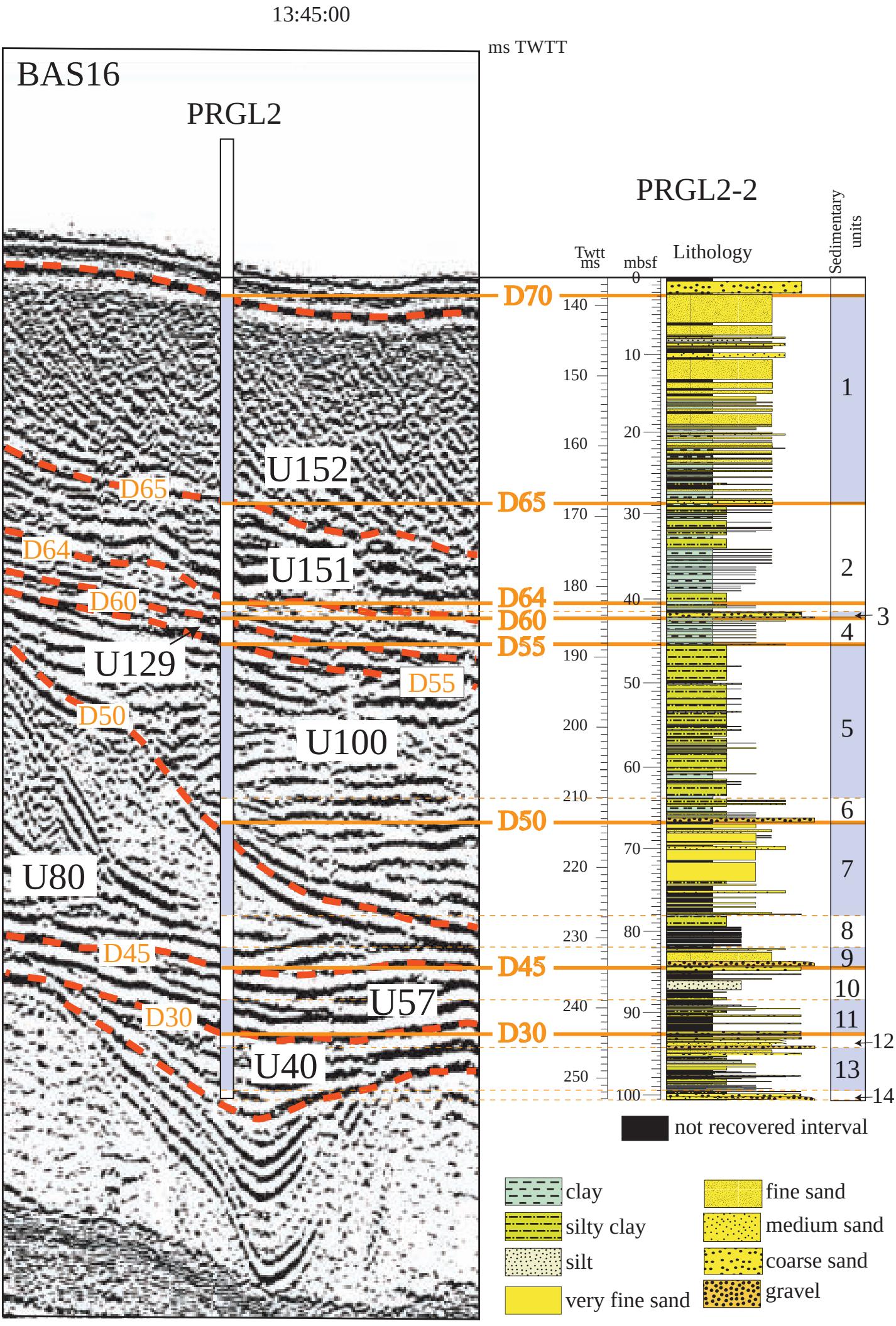

Figure 4_Bassetti et al._G3

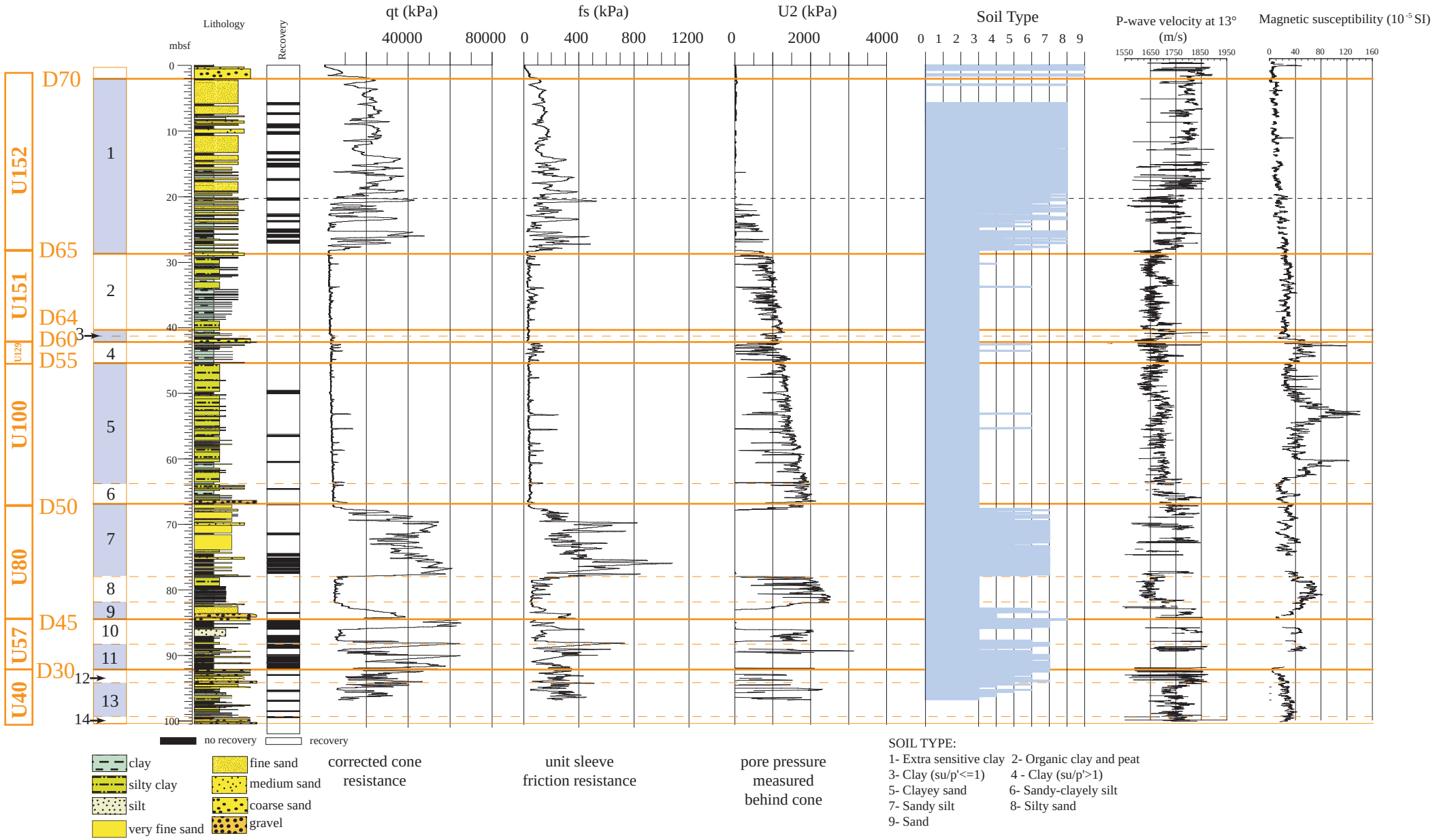

Figure 5_Bassetti et al._G3

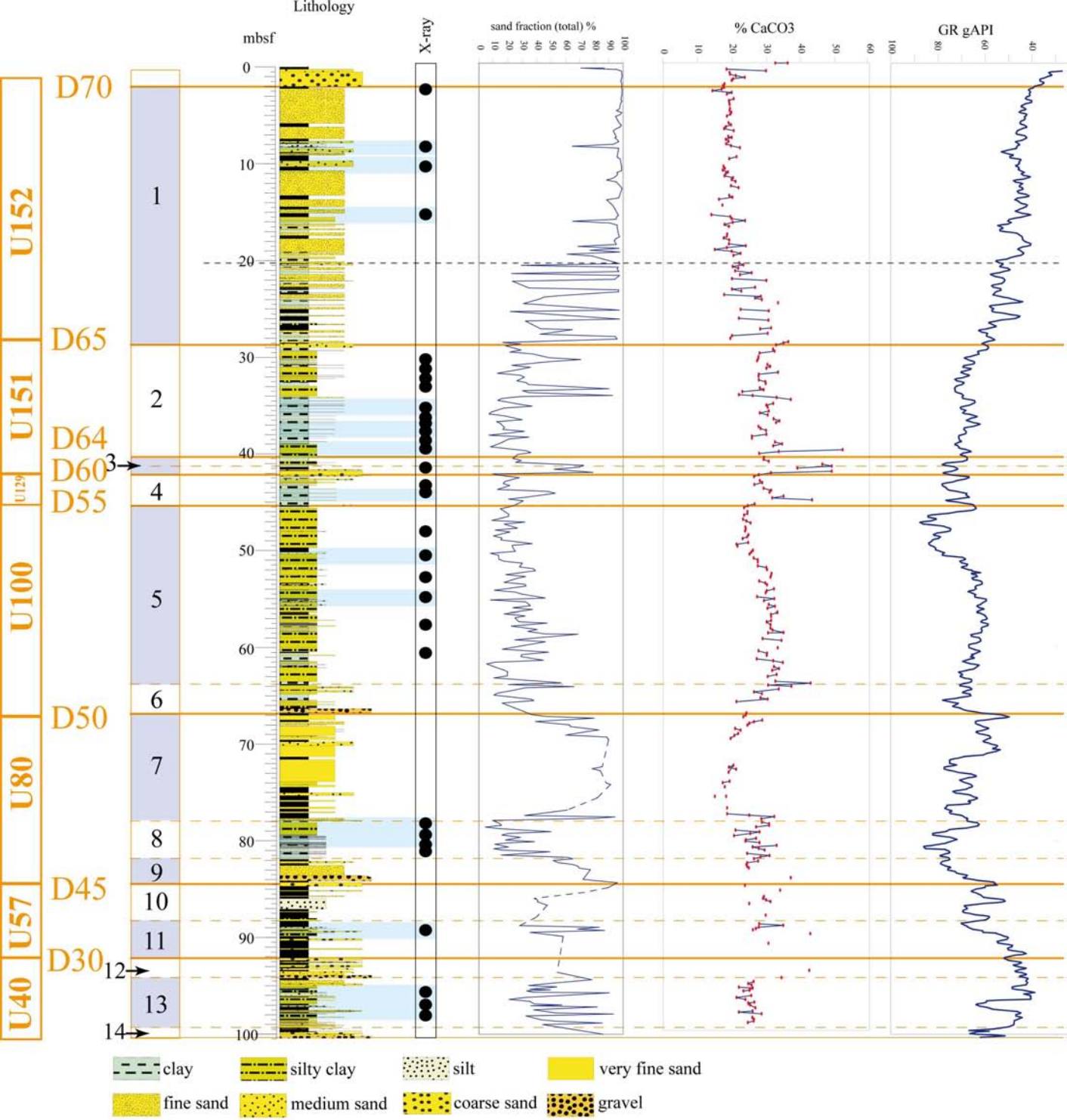

Figure 6_Bassetti et al._G3

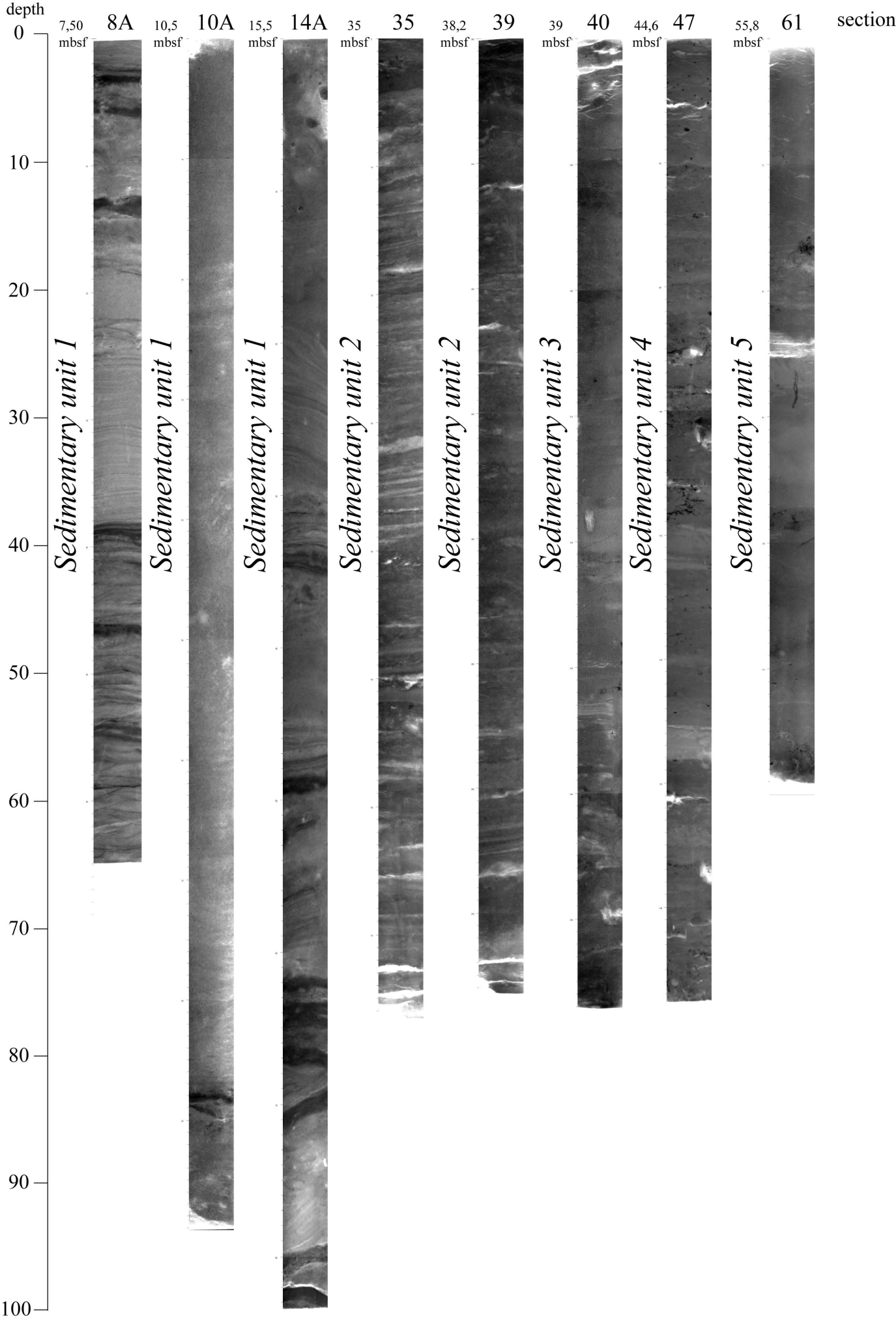

Figure 7_Bassetti et al._G3

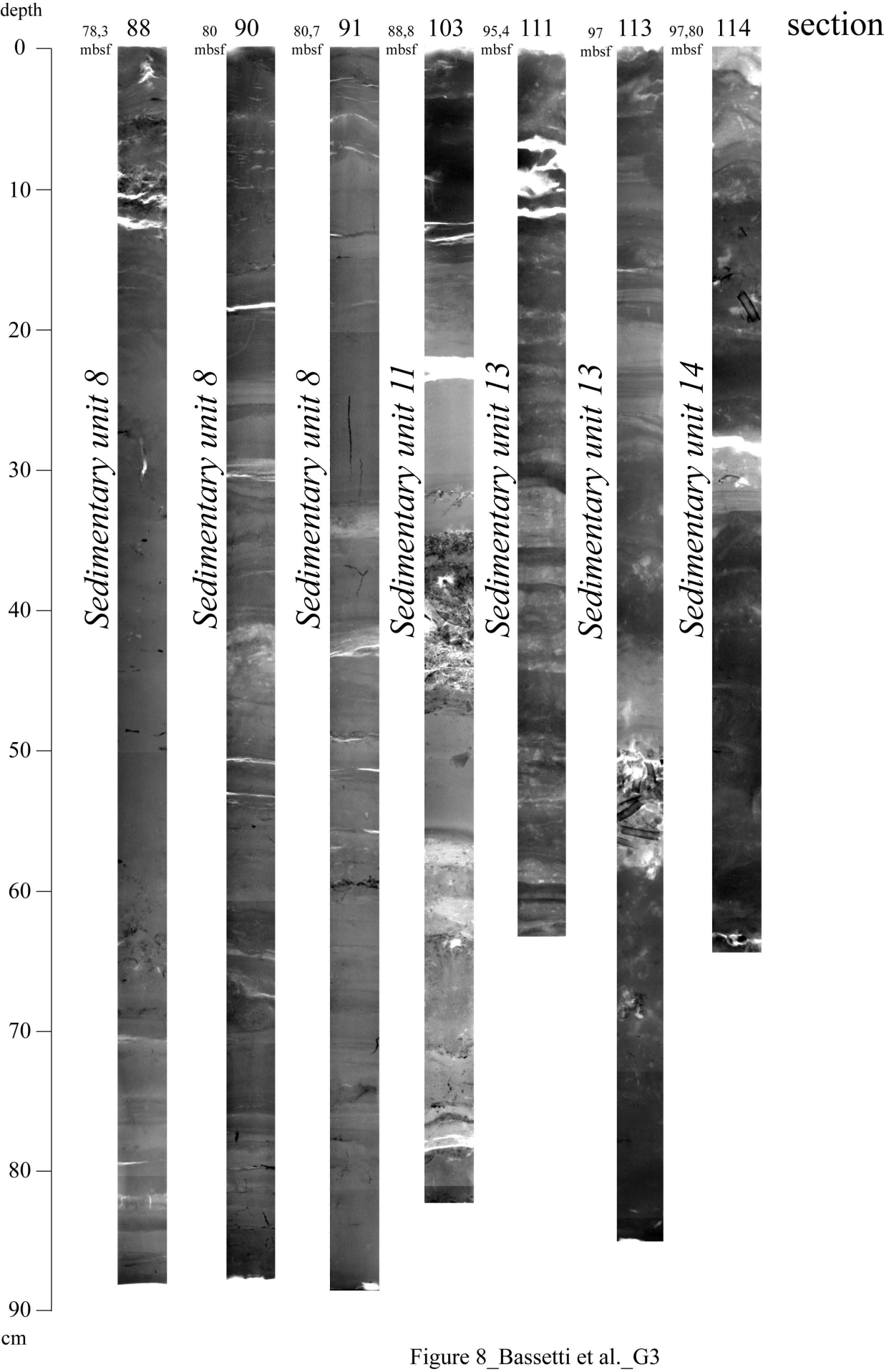

Figure 8_Bassetti et al._G3

Figure 9_Bassetti et al._G3

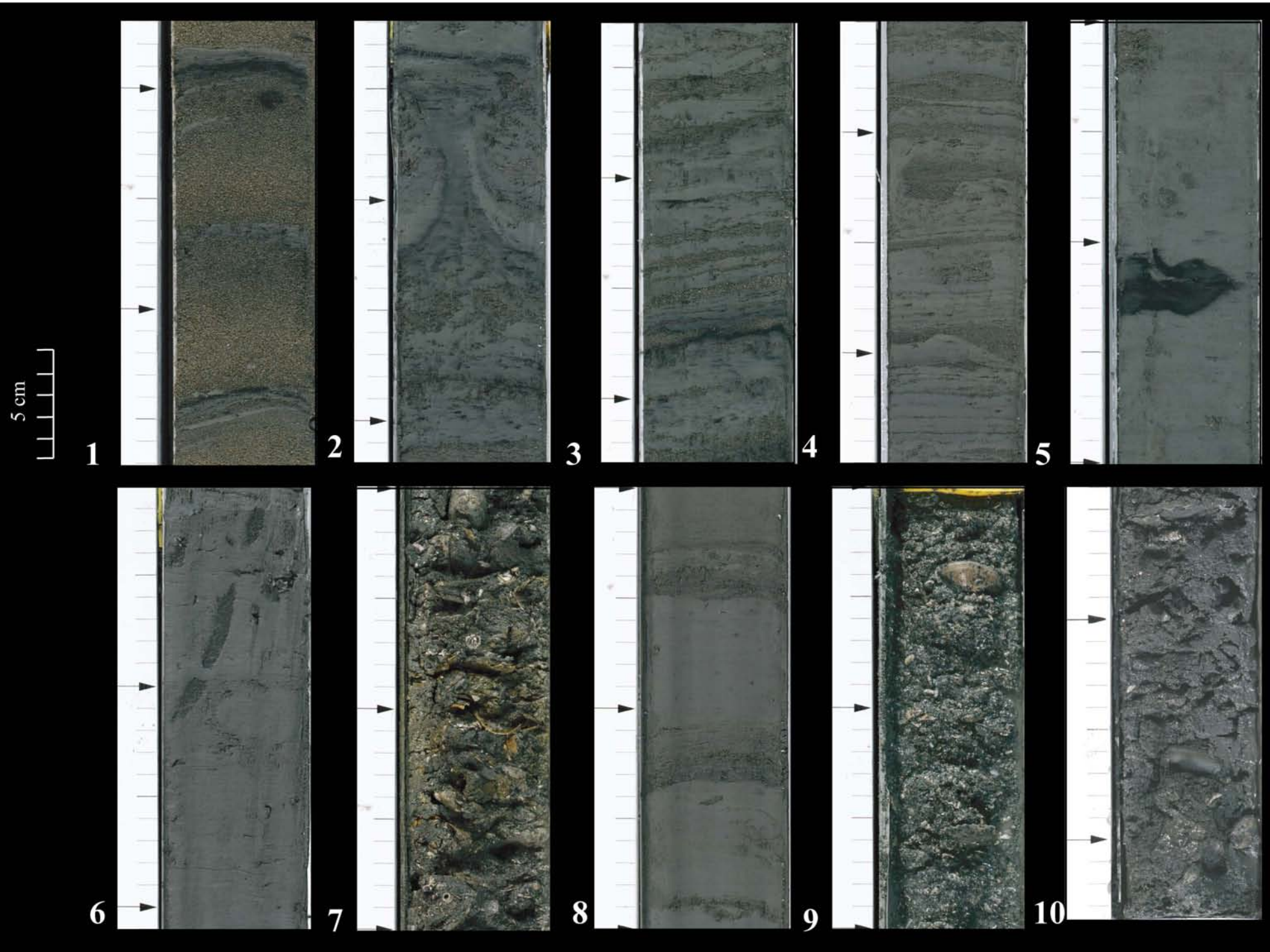

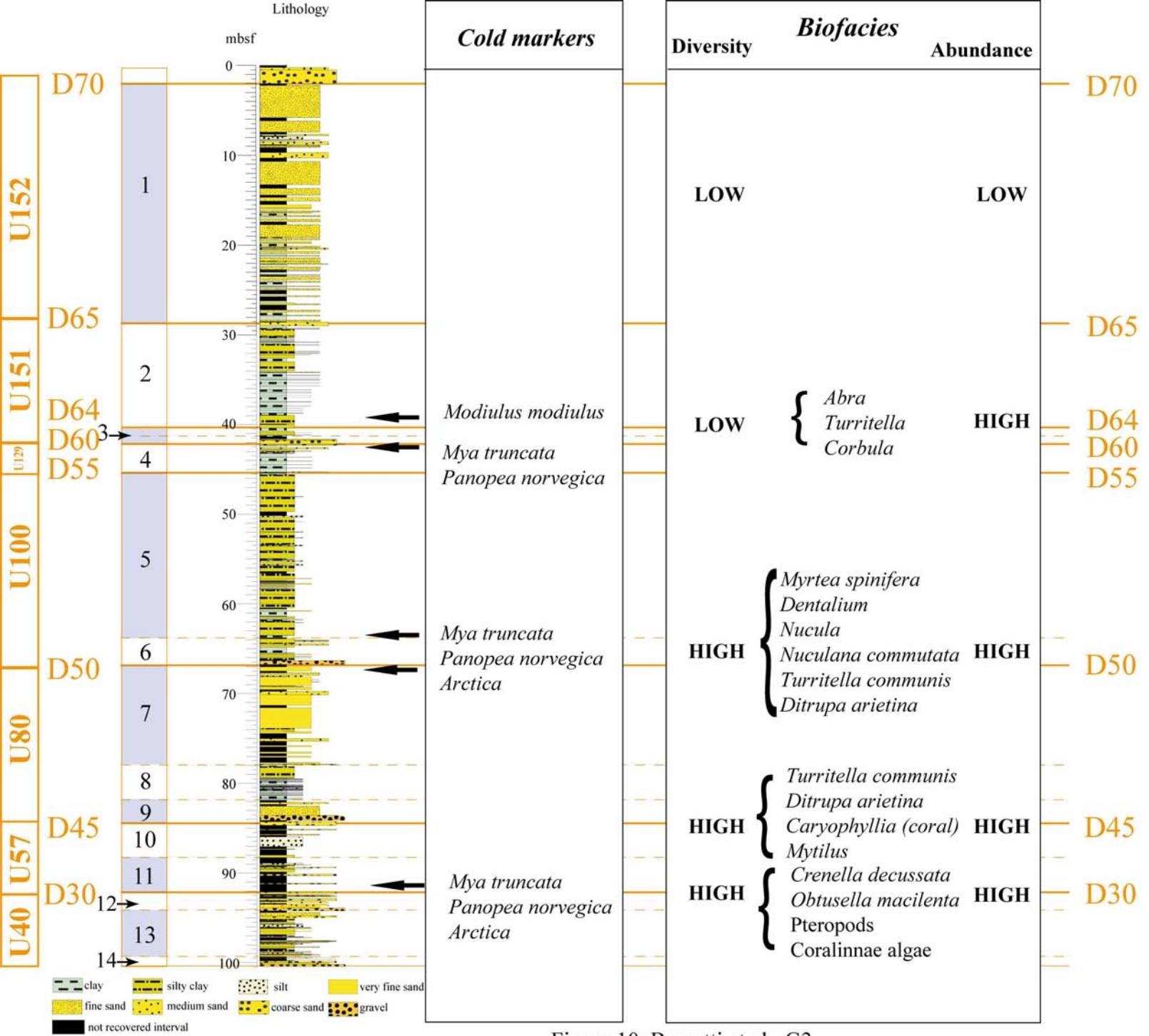

Figure 10_Bassetti et al._G3

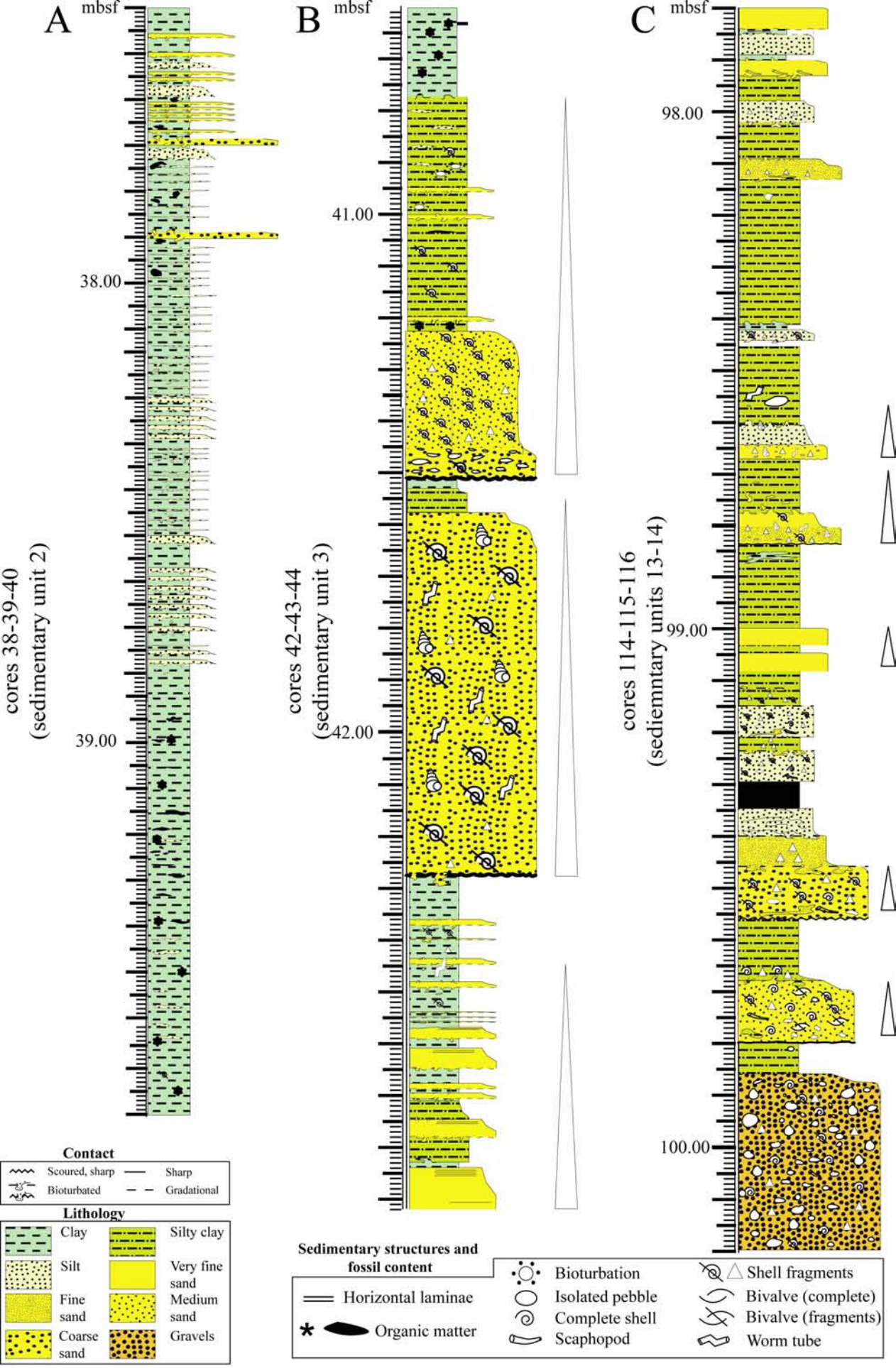

Figure 11_Bassetti et al_G3

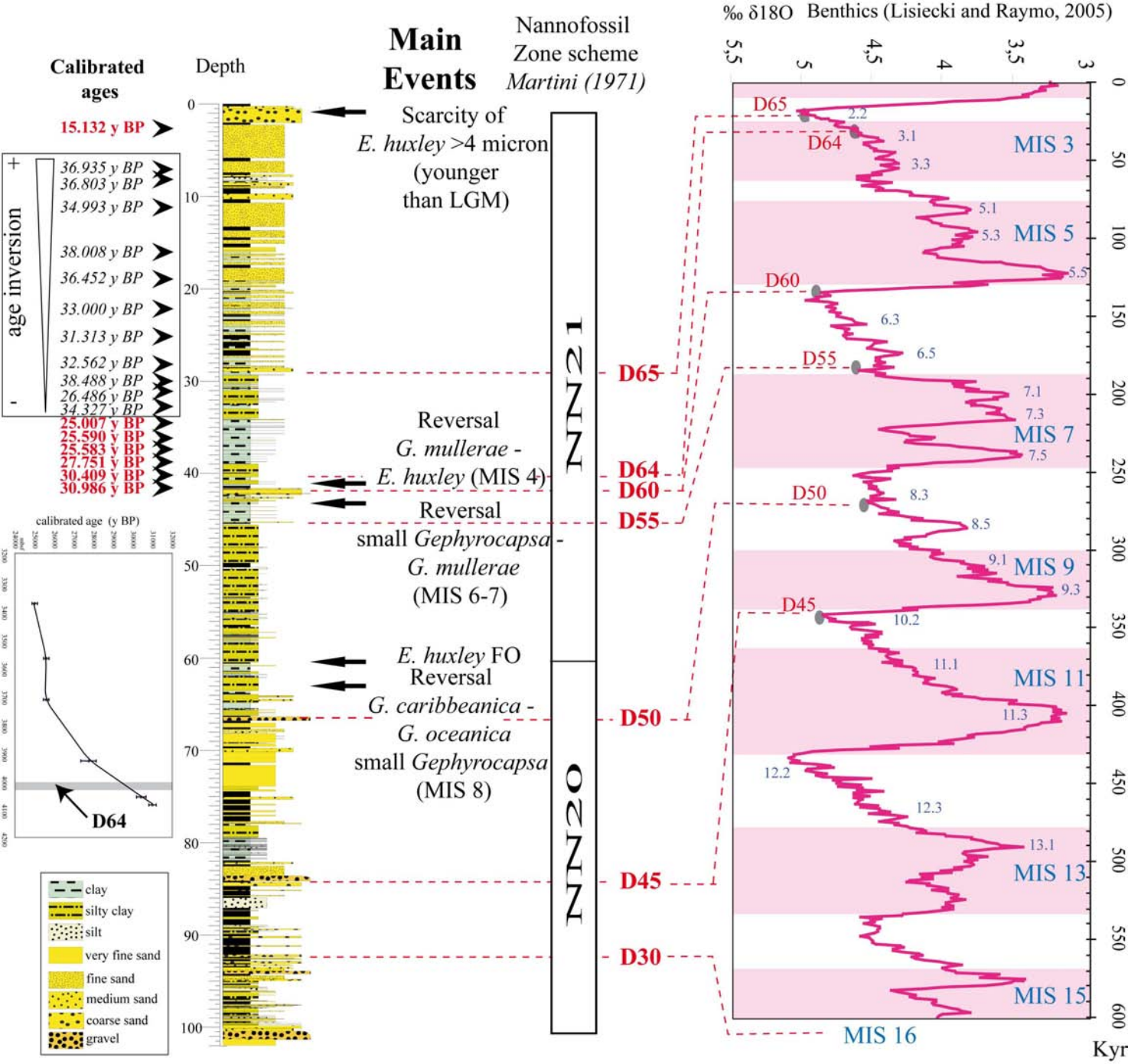

Figure 12_Bassetti et al._G3

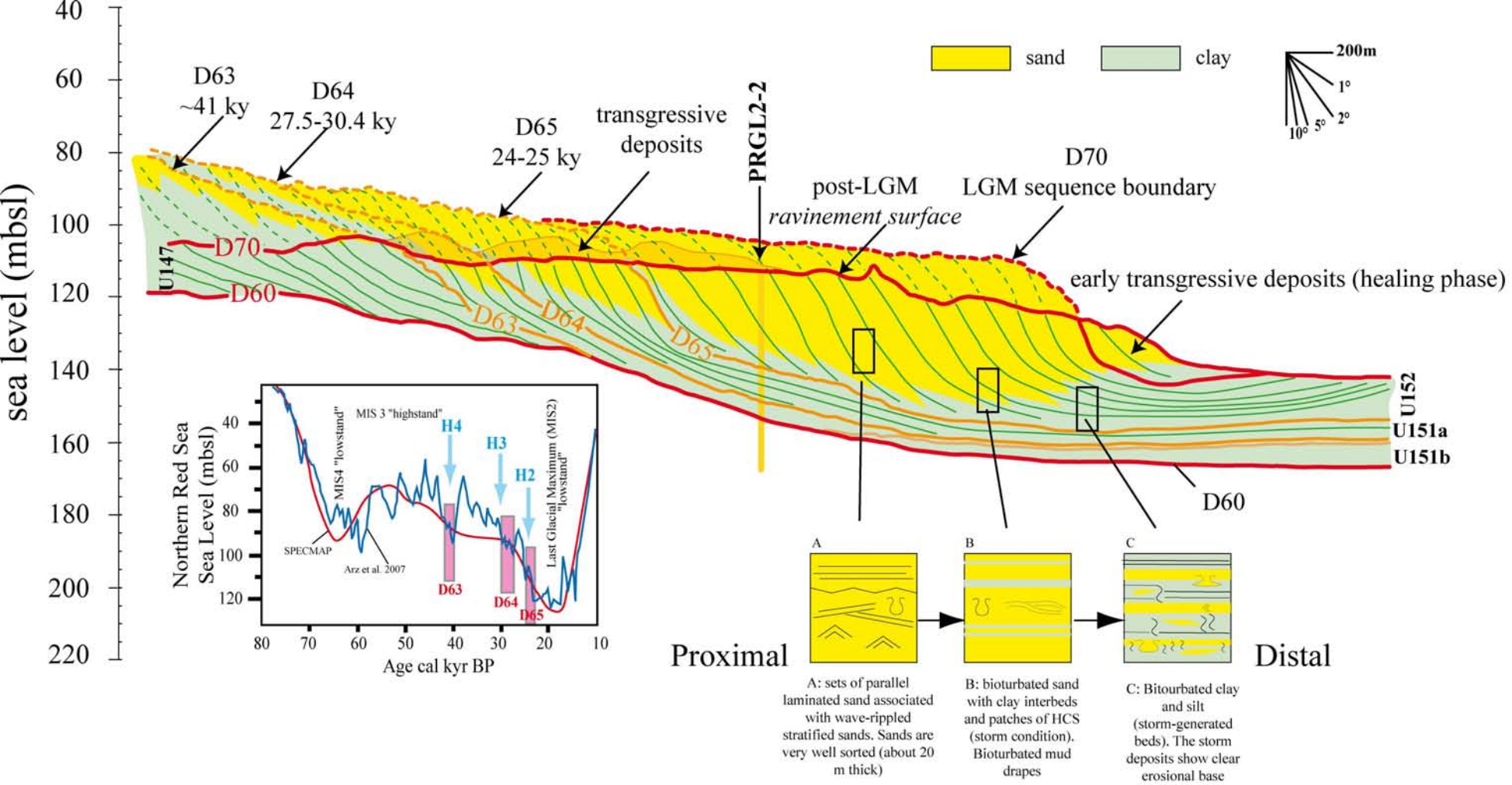

Figure 13_Bassetti et al._G3

APPENDIX A
MOLLUSC FAUNA COMPONENTS (PRGL2-2)

POLYPLACOPHORA
Leptochiton sp.

GASTROPODA
Acmaea unicolor
Acmaea sp.
Lepetella laterocompressa
Anatoma sp.
Calliostoma sp.
Gibbula magus
Gibbula sp.
Jujubinus sp.
Clelandella miliaris
Skeneidae sp.
Bittium sp.
Cerithidium submammillatum
Cerithidium sp.
Turritella communis
Turritella sp.
Rissoa sp.
Turboella sp.
Putilla sp.
Alvania cancellata
Alvania punctura
Alvania testae
Alvania sp.
Obtusella sp.
Rissoide sp.
Caecum trachea
Caecum sp.
Calyptraea chinensis
Capulus ungaricus
Euspira catena
Euspira sp.
Naticidae sp,
Epitonium sp.
Melanella sp.
Trophon muricatus
Trophon sp.
Buccinum undatum
Nassarius mutabils
Nassarius reticulates
Nassarius (Telasco) sp.
Nassarius sp.
Mitrella minor
Mitrella sp.
Bela brachystoma
Bela sp.
Raphitoma sp.
Teretia teres
Chrysallida, sp.
Eulimella sp.
Odostomia sp.
Pyramidellidae sp.
Actaeon tornatilis
Retusa truncatula
Retusa sp.
Ringicula auriculata
Cylichna cylindracea
Cylichna sp.
Diacria sp.
Creseis sp.
Limacina trochiformis
Limacina sp.
Substitute *Spiratella* sp.

BIVALVIA
Nucula sulcata
Nucula, sp.
Nuculana commutata
Nuculana sp.,
Arca sp.
Anadara corbuloides
Bathyarca grenophia,
Bathyarca sp.
Striarca lactea
Mytilus edulis/galloprovincialis
Crenella cf. *prideauxi*
Modiolus modiolus
Musculus sp.
Mytilidae sp.
Pecten jacobaeus
Aequipecten opercularis
Aequipecten sp.
Hyalopecten similis
Chlamys glabra
(=syn: Proteopecten glaber)
Chlamys sp.
Pectinidae spp,
Anomia, ephippium
Anomia sp.
Limatula sp.
Neopycnodonte cochlear
Ostreidae sp.
Lucinella divaricata
Myrtea spinifera
Diplodonta apicalis

Lasaeidae sp.
Leptonidae sp.
Mysella dentata
Mysella sp.
Montacutidae sp.
Neoleptonidae sp.
Glans aculeata
Astarte sulcata
Acanthocardia deshayesii
Acanthocardia echinata
Acanthocardia sp.
Parvicardium minimum
Parvicardium sp*,*
Plagiocardium papillosum
Laevicardium oblungum
Spisula subtruncata,
Spisula sp.
Tellina sp.
Gari fervensis
Abra alba
Abra prismatica,
Abra sp.
Arctica islandica
Venus casina
Chamelea gallina
Timoclea ovata
Dosinia lupinus
Dosinia sp.
Pitar rudis
Veneridae sp.
Mya truncata
Corbula gibba
Hiatella artica
Hiatella sp.
Thracia sp.
Pandora sp.

SCAPHOPODA
Dentalium inaequicostatum,
Dentalium sp.
Pulsellum lofotense

Auxiliary material for Paper 2007GC001854RRR

100-ky and rapid sea-level changes recorded by prograding shelf sand bodies in the Gulf of Lions (Western Mediterranean Sea)

M.A. Bassetti1,2, S. Berné1,2, G. Jouet2, M. Taviani3, B. Dennielou2, J.-A. Flores4, A. Gaillot5, R. Gelfort6, S. Lafuerza7, N. Sultan2
1Université de Perpignan IMAGES, 52 avenue Paul Alduy, Perpignan, France
2IFREMER, Géosciences Marines, BP70, 29280 Plouzané, France,
3ISMAR/CNR via Gobetti 101, Bologna, Italy
4Universidad de Salamanca, Facultad de Ciencias, Plaza Merced s/n, Salamanca, Spain
5NSE, BP70, 29280 Plouzané, France
6Institut für Geowissenschaftliche Gemeinschaftsaufgaben (GGA), Stilleweg 2, 30655, Hannover, Germany
7GRC Geociències Marines, Departament d'Estratigrafia i Paleontologia i Geociències Marines, Universitat de Barcelona, Martí i Franquès s/n, 08028 Barcelona, Spain
G-CUBED

Appendix B
Introduction
Stratigraphical distribution of Bivalvia and Gasteropoda in PRGL2-2

Bivalvia

D30, D40...= Erosional discontinuities (see Figure 4)

SU= Sedimentary Units (Table 1)

Unit	mbsf	section cm	*Nucula* sp.	*Nuculana* sp.	*Saccella commutata*	*Arca* sp.	*Anadara corbuloides*	*Bathyarca grenophia*	*Bathyarca* sp.	*Striarca lactea*	*Mitilus edulis galloprovincialis*	*Modiolus modiolus*	*Musculus* sp.	*Rhomboidella cf. prideauxi*	Mitilidae	*Limatula* sp.	*Neopycnodonte cochlear*	Ostreidae
D64	40.073	41/27-29										x						
	41.310	42/70-71	x															
	41.460	43/5-7	x															
	41.950	43/54-56																
D60	42.150	43/73-77	x		x		x	x										
	42.258	44/5-7	x		x			x										
	42.270	45/27-28																
	43.360	45/35-37																
D55	45.308	47/73-74																
	45.410	48/0-2																
	63.740	70/73-76	x									x						
D50	64.370	71/58-59	x											x				
	66.300	74/9-11																
	66.390	74/18-20																
	66.420	74/21-23																
	66.470	74/26-28	x		x		x	x										
	66.510	74/30-33	x		x			x				x						
	66.550	74/34-36	x		x			x				x						
	66.580	74/37-39		x								x						
	66.600	74/40-41			x							x						
	66.630	74/43	x		x				x			x						
	66.670	74/46-48			x				x			x						
	66.710	74/52-54			x							x						
	67.104	75/10-13										x						
	67.587	75/61-64																
SU7	69.150	78/3-8										x						
	69.180	78/7-9										x						
	69.290	78/18-20										x						
	69.500	78/40-41																
	69.750	78/64-66	x															
	69.800	78/69-71																
	78.358	88/7-8																
SU9	82.291	92 core shoe																
	83.600	95/bag1	x		x													
	83.660	95/bag2	x		x					x								
	83.600	95/0-2																
	83.620	95/7-9	x														x	
	83.640	95/9-10	x	x	x									x	x			x
	83.890	95/28-30												x				
	83.940	95/33-35												x			x	
D45	84.210	95/bottom	x		x	x	x	x							x			x
	84.520	96/12-13									x							
	86.145	96/17-18																
SU11	86.496	103/80-81																
	91.000	106/bag1																
	91.990	106/core bag	x							x				x				
	92.130	107A/12-14																
	92.210	107A/20-22																
	92.330	107B/10-12																
	92.410	107B/18-20																
	92.470	107B/24-26																
	92.570	107B/34-36																
D30	93.089	108/8-10																
	93.188	108/18-20																
	93.237	108/20-25																
SU12	93.514	108/51-53	x															
	93.612	108/61-63																
	93.960	109/16-17																
	93.080	109/28-29																
	94.400	109/60-61	x															
SU13	94.722	110/13-14																
	94.873	110/29-30		x											x			
	96.290	112/8-10																
	96.500	112/30																
	97.433	113/52-55																
	97.492	113/59-60																
	98.440	114/4																
	98.643	115/5-6	x										x					x
	98.745	115/17-18	x															
	98.898	115/35-36													x			
	98.915	115/37-38																
	99.068	115/55-56	x												x			
	99.162	115/65-67																
	99.230	115/73-75	x															
	99.332	115/85-87																
	99.504	116/11-13																
SU14	99.748	116/39-41																
	99.878	116/54-56														x		
	99.939	116/62-63																
	100.07	116/73-75																

mbsf	*Anomia ephippium*	*Anomia* sp.	*Pecten jacobaeus*	*Aequipecten opercularis*	*Aequipecten* sp.	*Chlamys* sp.	*Proteopecten glaber*	*Similipecten similis*	Pectinidae	*Acanthocardia deshayesii*	*Acanthocardia echinata*	*Acanthocardia* sp.	*Laevicardium oblongum*	*Parvicardium minimum*	*Parvicardium* sp.	*Plagiocardium papillosum*
40.073		x													x	
41.310									x							
41.460															x	
41.950																
42.150							x			x					x	
42.258									x						x	
42.270																x
43.360															x	
45.308															x	
45.410									x							
63.740															x	
64.370															x	
66.300												x				
66.390																
66.420							x									
66.470		x		x				x							x	
66.510							x								x	
66.550																
66.580		x													x	
66.600																
66.630		x													x	
66.670		x													x	
66.710															x	
67.104		x														
67.587																
69.150				x												
69.180																
69.290																
69.500	x															
69.750		x														
69.800																
78.358																
82.291													x			
83.600	x											x			x	
83.660		x		x											x	
83.600				x										x		
83.620	x					x									x	x
83.640	x			x						x				x		
83.890	x			x												
83.940	x								x					x		x
84.210		x		x							x			x		
84.520																
86.145																
86.496																
91.000				x								x				
91.990	x														x	
92.130															x	x
92.210		x														
92.330		x		x												
92.410																
92.470		x													x	
92.570		x										x				
93.089																
93.188				x												
93.237															x	
93.514		x		x		x						x				x
93.612																
93.960					x										x	
93.080	x															
94.400					x										x	
94.722															x	
94.873		x													x	x
96.290		x														
96.500		x												x		
97.433		x													x	
97.492																x
98.440		x														x
98.643	x		x	x								x			x	
98.745	x															
98.898		x													x	
98.915		x			x				x						x	x
99.068		x			x										x	
99.162		x														
99.230		x		x											x	
99.332		x		x											x	
99.504	x											x				
99.748	x					x								x		
99.878	x			x		x								x		
99.939					x										x	
100.07			x	x												

mbsf	*Lucinella divaricata*	*Myrtea spinifera*	Lasaeidae	Montacutidae	*Mysella bidentata*	*Mysella* sp.	Leptonidae	Neoleptonidae	*Tellina* sp.	*Abra alba*	*Abra prismatica*	*Abra* sp.	*Gari farvensis*	*Diplodonta apicalis*	*Glans aculeata*	*Astarte sulcata*
40.073																
41.310																
41.460																
41.950																
42.150										x						x
42.258																
42.270									x							
43.360																
45.308																
45.410												x				
63.740																
64.370																
66.300																
66.390																
66.420																
66.470												x				
66.510		x														
66.550																
66.580																
66.600		x														
66.630																
66.670																
66.710																
67.104																
67.587																
69.150																
69.180																
69.290																
69.500																
69.750																
69.800																
78.358																
82.291																
83.600																
83.660											x					
83.600																
83.620																
83.640									x			x				x
83.890																
83.940									x							
84.210													x		x	
84.520																
86.145																
86.496																
91.000																
91.990												x			x	
92.130																
92.210																
92.330																
92.410																
92.470																
92.570																
93.089																
93.188																
93.237																
93.514									x							
93.612														x		
93.960																
93.080																
94.400																
94.722																
94.873																
96.290																
96.500												x				
97.433										x						
97.492																
98.440																
98.643	x		x	x				x	x			x				
98.745																
98.898												x				
98.915							x					x				
99.068						x						x				
99.162																
99.230																
99.332																
99.504																
99.748					x				x							
99.878									x							
99.939																
100.07																

mbsf	*Arctica islandica*	*Spisula subtruncata*	*Spisula* sp.	*Chamelea gallina*	*Timoclea ovata*	*Venus casina*	*Pitar rudis*	*Dosinia lupinus*	*Dosinia* sp.	Veneridae	*Corbula gibba*	*Hiatella urtica*	*Hiatella* sp.	*Mya truncata*	*Pandora* sp.	*Thracia* sp.
40.073													x			
41.310					x											
41.460					x						x					
41.950					x					x						x
42.150					x	x				x	x					
42.258					x						x					
42.270																
43.360														x		
45.308																
45.410													x			
63.740																
64.370										x	x					
66.300					x											
66.390	x															
66.420	x															
66.470					x									x		
66.510					x				x		x				x	
66.550					x											
66.580					x											
66.600					x											
66.630					x	x							x			
66.670					x											
66.710					x											
67.104																
67.587	x															
69.150																
69.180																
69.290	x															
69.500																
69.750																
69.800														x		
78.358											x					
82.291								x								
83.600		x			x	x		x		x						
83.660			x		x				x							
83.600					x											
83.620					x					x						
83.640				x	x	x			x		x		x			
83.890				x												
83.940					x		x	x		x	x					
84.210					x	x			x	x	x		x			
84.520																
86.145	x															
86.496														x		
91.000	x				x				x							
91.990		x			x					x	x		x			
92.130	x				x					x						
92.210	x												x			
92.330													x	x		
92.410													x			
92.470					x											
92.570	x				x											
93.089																
93.188																
93.237	x									x						
93.514																
93.612														x		
93.960																
93.080					x											
94.400																
94.722																
94.873										x						
96.290														x		
96.500																
97.433					x								x			
97.492																
98.440					x											
98.643					x							x				
98.745																
98.898					x							x				
98.915					x						x		x			
99.068					x											
99.162													x			
99.230			x		x											
99.332					x								x			
99.504																
99.748		x								v	x					
99.878				x	x								x			
99.939																
100.07																

Gastropoda

D30, D40...= Erosional discontinuities (see Figure 4)

SU= Sedimentary Units (Table 1)

Unit	mbsf	section cm	*Anatoma* sp.	*Lepetella laterocompressa*	*Acmea unicolor*	*Acmea* sp.	*Globula magus*	*Gibbula* sp.	*Clelandella miliaris*	*Calliostoma* sp.	*Jujubinus* sp.	Skenidae	*Bittium* sp.	*Cerithidium submamillatum*	*Cerithidium* sp.	*Rissoa* sp.	*Turboella* sp.	*Alvania cancellata*
D64	40.073	41/27-29																
	41.310	42/70-71																
	41.460	43/5-7			x													
	41.950	43/54-56																
D60	42.150	43/73-77																
	42.258	44/5-7			x													
	42.270	45/27-28																
	43.360	45/35-37																
D55	45.308	47/73-74																
	45.410	48/0-2																
	63.740	70/73-76																
D50	64.370	71/58-59											x					
	66.300	74/9-11																
	66.390	74/18-20																
	66.420	74/21-23																
	66.470	74/26-28																
	66.510	74/30-33																
	66.550	74/34-36																
	66.580	74/37-39																
	66.600	74/40-41																
	66.630	74/43			x												x	
	66.670	74/46-48																
	66.710	74/52-54																
	67.104	75/10-13																
	67.587	75/61-64																
SU7	69.150	78/3-8																
	69.180	78/7-9																
	69.290	78/18-20																
	69.500	78/40-41																
	69.750	78/64-66																
	69.800	78/69-71																
	78.358	88/7-8																
SU9	82.291	92 core shoe																
	83.600	95/bag1					x											
	83.660	95/bag2								x							x	
	83.600	95/0-2																
	83.620	95/7-9																
	83.640	95/9-10			x					x			x	x				x
	83.890	95/28-30																
	83.940	95/33-35	x						x									
D45	84.210	95/bottom		x													x	
	84.520	96/12-13																
	86.145	96/17-18																
SU11	86.496	103/80-81																
	91.000	106/bag1						x										
	91.990	106/core bag			x		x	x					x	x		x		x
	92.130	107A/12-14																
	92.210	107A/20-22			x			x										
	92.330	107B/10-12									x							
	92.410	107B/18-20						x										
	92.470	107B/24-26				x		x										
	92.570	107B/34-36						x										
D30	93.089	108/8-10						x										
	93.188	108/18-20											x					
	93.237	108/20-25						x					x					
SU12	93.514	108/51-53						x										x
	93.612	108/61-63						x										
	93.960	109/16-17																
	93.080	109/28-29									x					x		
	94.400	109/60-61						x					x					
SU13	94.722	110/13-14						x										
	94.873	110/29-30											x					
	96.290	112/8-10																
	96.500	112/30						x										
	97.433	113/52-55			x			x										
	97.492	113/59-60																
	98.440	114/4						x										
	98.643	115/5-6						x				x	x		x	x		
	98.745	115/17-18																
	98.898	115/35-36						x										
	98.915	115/37-38			x			x					x					
	99.068	115/55-56						x					x					
	99.162	115/65-67						x										
	99.230	115/73-75						x					x					
	99.332	115/85-87						x					x					
	99.504	116/11-13						x			x		x					
SU14	99.748	116/39-41			x											x		
	99.878	116/54-56			x			x										
	99.939	116/62-63			x			x										
	100.07	116/73-75			x													

mbsf	*Alvania punctura*	*Alvania testae*	*Alvania* sp.	*Obtusella* sp.	*Putilla* sp.	*Rissoide* sp.	*Caecum trachea*	*Caecum* sp.	*Turritella communis*	*Turritella* sp.	*Calyptraea chinensis*	*Capulus ungaricus*	*Euspira catena*	*Euspira* sp.	*Naticidae* sp.	*Epitonium* sp.
40.073																
41.310										x				x		
41.460		x							x		x					
41.950		x							x							
42.150		x							x							
42.258									x							
42.270																
43.360																
45.308																
45.410																
63.740																
64.370																
66.300									x							
66.390									x							
66.420																
66.470									x							
66.510		x							x		x					
66.550		x							x							
66.580										x						
66.600		x											x			
66.630		x							x					x		
66.670									x							
66.710		x														
67.104																
67.587																
69.150									x							
69.180																
69.290																
69.500																
69.750																
69.800																
78.358																
82.291																
83.600	x								x			x		x		
83.660		x							x		x			x		
83.600									x						x	
83.620									x							
83.640		x	x	x					x			x		x		
83.890																
83.940	x								x		x				x	
84.210		x				x			x			x		x		
84.520				x					x							
86.145																
86.496																
91.000									x		x			x		
91.990			x	x			x		x		x			x		
92.130				x					x							
92.210													x			
92.330										x						
92.410				x					x							
92.470				x				x			x					
92.570										x	x					
93.089																
93.188																
93.237				x						x						
93.514				x				x	x		x					
93.612											x					
93.960				x					x							
93.080				x					x							
94.400				x					x							
94.722									x		x					
94.873									x							
96.290									x							
96.500				x							x					
97.433					x											
97.492																
98.440			x		x											
98.643			x						x		x				x	x
98.745					x					x						
98.898					x	x				x	x					
98.915					x						x					
99.068					x						x					
99.162										x						
99.230					x				x							
99.332					x						x					
99.504										x						
99.748					x						x					
99.878	x				x			x			x			x		
99.939																
100.07											x					

mbsf	*Melanella* sp.	*Trophonopsis muricatus*	*Trophon* sp.	*Buccinum undatum*	*Nassarius mutabilis*	*Nassarius reticulatus*	*Nassarius* sp.	*Nassarius (telasco)*	*Mitrella minor*	*Mitrella* sp.	*Bela brachystoma*	*Bela* sp.	*Raphitoma* sp.	*Teretia teres*	*Chrysallida* sp.	*Eulimella* sp.
40.073																
41.310																
41.460																
41.950																
42.150		x														
42.258		x					x									
42.270				x												
43.360																
45.308																
45.410																
63.740																
64.370			x													
66.300																
66.390																
66.420																
66.470																x
66.510																
66.550																
66.580													x			
66.600																
66.630	x						x				x					
66.670																
66.710																
67.104																
67.587																
69.150																
69.180																
69.290																
69.500																
69.750																
69.800																
78.358																
82.291																
83.600		x				x	x	x	x		x				x	
83.660						x	x	x	x		x				x	
83.600								x			x					
83.620					x			x		x			x			
83.640		x					x	x	x		x					x
83.890								x								
83.940							x						x			
84.210		x					x			x	x			x		
84.520																
86.145																
86.496																
91.000							x									
91.990		x					x								x	
92.130																
92.210																
92.330		x														
92.410							x								x	
92.470																
92.570							x									
93.089																
93.188							x									
93.237		x														
93.514							x					x				
93.612																x
93.960																
93.080					x											
94.400															x	
94.722											x	x				
94.873																
96.290																
96.500																
97.433																
97.492																
98.440																
98.643															x	
98.745																
98.898																
98.915																
99.068						x										
99.162																
99.230																
99.332							x									
99.504																
99.748		x														
99.878							x								x	
99.939																
100.07																

	Gastropoda												1			2
mbsf	*Odostomia* sp.	Pyramidellidae	*Cylichna cylindracea*	*Cylichna* sp.	*Retusa truncatula*	*Retusa* sp.	*Acteon tornatilis*	*Ringicula auriculata*	*Creseis* sp.	*Diacria* sp. *(Pteropod)*	*Limacina throchiformis*	*Spiratella* sp.	*Dentalium* sp.	*Antalis aequicostatum*	*Pulsellum lofotense*	*Leptochiton* sp.
40.073																
41.310																
41.460																
41.950																
42.150	x															
42.258																
42.270																
43.360																
45.308																
45.410																
63.740																
64.370																
66.300																
66.390																
66.420																
66.470													x			
66.510																
66.550													x			
66.580						x										
66.600																
66.630																
66.670																
66.710																
67.104	x															
67.587																
69.150																
69.180																
69.290																
69.500																
69.750																
69.800																
78.358																
82.291																
83.600	x		x	x										x		
83.660	x															x
83.600		x	x													
83.620																
83.640	x			x			x									
83.890														x		
83.940										x			x			
84.210				x				x	x					x	x	
84.520																
86.145																
86.496																
91.000																
91.990				x												
92.130																
92.210																
92.330																
92.410																
92.470																
92.570																
93.089																
93.188																
93.237	x															
93.514	x															x
93.612																
93.960																
93.080										x						
94.400																
94.722													x			
94.873																
96.290																
96.500																
97.433																
97.492																
98.440																
98.643					x						x		x			
98.745					x											
98.898												x				
98.915						x						x				
99.068		x			x											
99.162																
99.230		x														
99.332												x				x
99.504																
99.748	x															
99.878												x				
99.939																
100.07																

1= Scapophoda 2= Polyplacophora

Auxiliary material for Paper 2007GC001854RRR

100-ky and rapid sea-level changes recorded by prograding shelf sand bodies in the Gulf of Lions (Western Mediterranean Sea)

M.A. Bassetti1,2, S. Berné1,2, G. Jouet2, M. Taviani3, B. Dennielou2, J.-A. Flores4, A. Gaillot5, R. Gelfort6, S. Lafuerza7, N. Sultan2

1Université de Perpignan IMAGES, 52 avenue Paul Alduy, Perpignan, France

2IFREMER, Géosciences Marines, BP70, 29280 Plouzané, France,

3ISMAR/CNR via Gobetti 101, Bologna, Italy

4Universidad de Salamanca, Facultad de Ciencias, Plaza Merced s/n, Salamanca, Spain,

5NSE, BP70, 29280 Plouzané, France

6Institut für Geowissenschaftliche Gemeinschaftsaufgaben (GGA), Stilleweg 2, 30655, Hannover, Germany

7GRC Geociències Marines, Depart. d'Estratigrafia i Paleontologia i Geociències Marines, Univ. de Barcelona, Martí i Franquès s/n, 08028 Barcelona, Spain

G-CUBED

Table 1

Introduction

This table summarises the definition of sedimentary units recognized in the PRGL2-2 borehole. The core number appears in the first column, followed by the corresponding depth in meter below sea floor (second column). Synthetic description of lithology and the equivalence with seismic facies are given in the fourth and fifth columns.

Core number	mbsf	Unit	Facies description	Seismic expression	Environment/deposits
2-27	0-28.75	**1**	Fine-very fine grained sand, well sorted and homogeneous with rare pebbles and shells. Mud interbeds. Planar lamination, tabular cross-bedding	Oblique reflectors with truncated topsets	Foreshore-upper shoreface
27-42/43	28.75-41.51	**2**	Silt-mud couplets (mm thick), intensively bioturbated. The silt laminae do not show gradation and have sharp (erosional) bases and tops	Tangential reflectors downlapping seawards	Lower shoreface-offshore transition
43-44	41.51-42.32	**3**	Coarse grained, muddy sand with abundant shells (fragments)	Planar scour surface	Basal *ravinement* Submarine erosion
44-47	42.32-45.41	**4**	Clay-silt couplets with spare bioturbation and organic matter. Scattered shell debris. The interval is based by coarse, bioclastic sand	Planar reflectors, onlapping landwards	Minor lobe of distibutary channel
48-70	45.41-63.60	**5**	Dark grey silty clay, with rare sand interbeds. Sparse organic matter and shell debris.	Undulated reflectors	Sediment waves
70-74	63.60-66.80	**6**	Very coarse-grained muddy sand, mixed with pebbles. Abundant and well preserved shells.	Planar scour surface	Basal *ravinement* Submarine erosion
74-87	66,80-77.80	**7**	Fine-very fine grained sand, well sorted and homogeneous with rare pebbles and shells. Mud interbeds. Planar lamination, tabular cross-bedding	Oblique reflectors with toplap terminations below a planar scour	Foreshore-upper shoreface
87-91	77.80-81.40	**8**	Mud-sand alternations. The sand horizons show horizontal lamination and they are intensively bioturbated	Tangential reflectors downlapping seawards	Lower shoreface-offshore
92-96	81.40-84.4	**9**	Poorly sorted sand with abundant biogenic material *Poor recovery between 84.50 and 86.00 mbsf*- medium-coarse grained sand with shell debris	Planar scour surface	Basal *ravinement* Submarine erosion
96-102	84.40-88.28	**10**	Silty clay-sand alternations with rare shell fragments and scattered pebbles	Convex, parallel reflectors	Mouth bar
103-107B	88.28-92.37	**11**	Strongly heterogeneous and containing abundant shell fragments. Roughly graded coarse grained intervals at the top	Parallel reflectors	Mouth bar, debris flow deposits
107B-109	92.37-94.15	**12**	Very coarse-grained deposits	Parallel reflectors	Basal *ravinement* Submarine erosion
109-115	94.15-99.24	**13**	Alternating coarse to fine-grained graded sand beds and burrowed silty clay	Concave, parallele reflectors	Mouth bar, debris flow deposits
115-116	99.24-100.13	**14**	Very coarse clastic material made of large rounded clasts and abundant shell fragments passing upwards to roughly grades coarse sand bes	Concave, parallele reflectors	Channel infill

Auxiliary material for Paper 2007GC001854RRR

100-ky and rapid sea-level changes recorded by prograding shelf sand bodies in the Gulf of Lions (Western Mediterranean Sea)

M.A. Bassetti1,2, S. Berné1,2, G. Jouet2, M. Taviani3, B. Dennielou2, J.-A. Flores4, A. Gaillot5, R. Gelfort6, S. Lafuerza7, N. Sultan2

1Université de Perpignan IMAGES, 52 avenue Paul Alduy, Perpignan, France

2IFREMER, Géosciences Marines, BP70, 29280 Plouzané, France,

3ISMAR/CNR via Gobetti 101, Bologna, Italy

4Universidad de Salamanca, Facultad de Ciencias, Plaza Merced s/n, Salamanca, Spain,

5NSE, BP70, 29280 Plouzané, France

6Institut für Geowissenschaftliche Gemeinschaftsaufgaben (GGA), Stilleweg 2, 30655, Hannover, Germany

7GRC Geociències Marines, Depart. d'Estratigrafia i Paleontologia i Geociències Marines, Univ. de Barcelona, Martí i Franquès s/n, 08028 Barcelona, Spain

G-CUBED

Table 2

Introduction

Table showing the 14C dates carried out in the PRGL2-2 borehole.

First column indicates sample position in the core, followed by sample weight, type of material and dating technique.

The last three columns show the conventional ages, reservoir age and the calibration procedure.

core	sample depth (cm)	sample weight (mg)	Material	dating technique	Conventional C14 age (BP)	reservoir age	calibrated ages (y BP)	calibration reference	calibration curve
PRGL2-2-4A 60-61	252.0-252.9	49	bivalve	AMS	13220 ± 60	400	14998-15240 **(15132)**	Hughen et al. (2004)	calib5_1 marine04.1
PRGL2-2-7 100-101	700.0-701.0	12	benthic Foraminifera (*Elphidium+Ammonia)*	AMS	31780 ± 320	400	36584-37287 **(36935)**	Bard et al. (1998) Glacial polynomial	
PRGL2-2-8A 40-41	790.0-791.0	18	benthic Foraminifera (*Elphidium+Ammonia*)	AMS	31660 ± 310	400	36463-37144 **(36803)**	Bard et al. (1998) Glacial polynomial	
PRGL2-2-10A 80-81	1128.0-1129.0	16	benthic Foraminifera (*Elphidium+Ammonia*)	AMS	30020 ± 260	400	34705-35282 **(34993)**	Bard et al. (1998) Glacial polynomial	
PRGL2-2-14A 60-61	1610.0-1611.0	33	benthic Foraminifera (*Elphidium*)	AMS	32760 ± 340	400	37637-38380 **(38008)**	Bard et al. (1998) Glacial polynomial	
PRGL2-2-16A 80-81	1930.0-1931.0	42	benthic Foraminifera (*Elphidium*)	AMS	31340 ± 300	400	36122-36782 **(36452)**	Bard et al. (1998) Glacial polynomial	
PRGL2-2-18 60-61	2190.0-2191.0	23	benthic Foraminifera (*Elphidium*)	AMS	28230 ± 220	400	32753-33246 **(33000)**	Bard et al. (1998) Glacial polynomial	
PRGL2-2-23 08-09	2548.0-2549.0	32	benthic Foraminifera (*Elphidium*)	AMS	26730 ± 190	400	31099-31528 **(31313)**	Bard et al. (1998) Glacial polynomial	
PRGL2-2-26 70-71	2840.9-2841.7	30	benthic Foraminifera (*Elphidium*)	AMS	27840 ± 210	400	32327-32798 **(32562)**	Bard et al. (1998) Glacial polynomial	
PRGL2-2-29 08-09	3028.0-3029.0	4600	Total Organic Carbon (TOC)	AMS	33200 ± 500	400	37944-39033 **(38488)**	Bard et al. (1998) Glacial polynomial	
PRGL2-2-29 58-59	3078.0-3079.0	14	benthic Foraminifera (*Elphidium*)+ 1 juvenil valve	AMS	22500 ± 150	400	26313-26659 **(26486)**	Bard et al. (1998) Glacial polynomial	
PRGL2-2-32 21-22	3279.5-3280.5	4520	Total Organic Carbon (TOC)	AMS	29420 ± 330	400	33960-34694 **(34327)**	Bard et al. (1998) Glacial polynomial	
PRGL2-2-33 31.5-37	3371.5-3378.0	24	2 valves of one bivalve	AMS	21190 ± 140	400	24786-25332 **(25007)**	Hughen et al. (2004)	calib5_1 marine04.1 4c
PRGL2-2-34 09-12	3429.0-3432.0	14	benthic Foraminifera (*Elphidium+Ammonia*)	AMS	29560 ± 250	400	34205-34761 **(34383)**	Bard et al. (1998) Glacial polynomial	
PRGL2-2-35 67.5-68.5	3567.5-3568.5	5700	Total Organic Carbon (TOC)	AMS	28720 ± 310	400	33201-33893 **(33547)**	Bard et al. (1998) Glacial polynomial	
PRGL2-2-35 68.5-70	3568.5-3570.0	9,5	Foraminifera	AMS	21590 ± 150	400	25407-25742; 25876-26000 **(25590)**	Hughen et al. (2004)	calib5_1 marine04.1 4c
PRGL2-2-36 58	3638	10	Wood	AMS	17480 ± 250	400	19933-20448 **(20216)**	Hughen et al. (2004)	calib5_1 marine04.1 4c
PRGL2-2-37 50-59	3710.0-3719.0	16,6	Foramifera	AMS	22120 ± 120	400	25445-25722 **(25583)**	Bard et al. (1998) Glacial polynomial	
PRGL2-2-38 65-66	3805.0-3806.0	5700	Total Organic Carbon (TOC)	AMS	27330 ± 260	400	31245-31832 **(31538)**	Bard et al. (1998) Glacial polynomial	
PRGL2-2-40 30-35	3930.0-3935.0	11,02	Foraminifera	AMS	24000 ± 500	400	27177-28325 **(27751)**	Bard et al. (1998) Glacial polynomial	
PRGL2-2-41 CS	>4055.1 and ≤4060.0	17,36	Foramifera	AMS	26330 ± 200	400	30182-30636 **(30409)**	Bard et al. (1998) Glacial polynomial	
PRGL2-2-42 25-30	4085.0-4090.0	1110	Shell: *Astarte sulcata*	AMS	26840 ± 170	400	30794-31178 **(30986)**	Bard et al. (1998) Glacial polynomial	